Master thesis in

Materials, Energy and Nanotechnology

Upconverting nanorods in silica film for use in CO_2 -optodes

Synthesis and characterization of
β-$NaYF_4$:Yb,Er

60 credits

Department of Physics

Faculty of Mathematics and Natural Sciences

UNIVERSITY OF OSLO

Live Karine Næss Killingland

May 22nd 2015

PREFACE

First of all I would like to thank my supervisors Jaan Roots and Peyman Muntaheri for making this project possible. The more I have come to learn about upconverting materials, the more fascinated I have become, and I am happy to have been introduced to the field.

What I consider as the most important help I have got during this project, although it might seem trivial, is by Per Anders Hansen who handed me the commercial sample of $NaYF_4$:Yb,Er. This allowed me to test the laser drive and lasers and understand what type of signal I could expect from my own samples. Thank you.

I would like to thank the staff at the University of Oslo who have helped me with the characterizations of the material, in particular Kristian Blindheim Lausund, Spyros Diplas, Sissel Jørgensen, Phuong Dan Nguyen and Øystein Prytz

Finally I would like to thank Magne Kringberg who has always been available for questions, and the students of my class whom have made my time at the University a special one.

A last remark is that all illustrations are made by the author.

Happy reading,

Live Karine Næss Killingland

University of Oslo, May 22nd 2015

ABSTRACT

The upconverting material of β-$NaYF_4$:Yb,Er powder has been successfully made by a solvothermal syntheses method. The morphology of the main sample is hexagonal rods of about 1.2 µm in length. The samples show visible green upconversion by IR excitation at 980 nm.

Four different syntheses methods were applied, and the final one developed by the author showed the most uniform particles. The samples were characterized by SEM, XRD and optical spectroscopy. 210^0C and 24h proved to be the ideal synthesis parameters for producing the material together with the surfactant oleic acid. Oleylamine was also investigated as a surfactant, however to poor results.

SEM and XRD investigations show that there is also NaF present in the samples. Unfortunately the optical measurements do not support the observed luminescence for all of the samples. This can be assigned as a result of scattering or absorption of both the laser and the emission of the material by NaF. The poor colloidal stability of the samples in cyclohexane should also be remarked upon.

Furthermore the heat-up strategy for producing core-shell particles of β-$NaYF_4$:Yb,Er@β-$NaYF_4$:Nd was investigated and the samples briefly investigated by TEM and XPS as well as SEM and XRD. The results indicate a core-shell structure, however further studies are needed. The optical spectroscopy results are inconclusive for IR excitation at 808 nm. However, it can be observed that the samples still show green luminescence by excitation at 980 nm.

Finally the particles were tried incorporated in a sensing element of silica also containing the chromophore BTB. The sol-gel synthesis of the film was not successful and the $NaYF_4$:Yb,Er powder was not compatible with the sol. A sensing element of silica with CP was successfully made which also showed a sensitivity towards dissolved CO_2 in water.

ABBREVIATIONS

Abbreviation	Full name or explanation
@	Indicates a core-shell structure
BSE	Backscattered electrons
BTB	Bromethyl blue
BTB-TOA	Ionpair of Bromethyl blue and TOAOH
c.h	Cyclohexane
CP	Cresol purple
CP-ODA	Ionpair of Cresol purple and ODAOH-TMOS
C3-TMOS	n-propyl-trimetoxysilane
E_B	Binding energy
EDS	Energy dispersive spectroscopy
E_K	Kinetic energy
Er^{3+}	Erbium ion
ESA	Excited state absorption
EtOH	Ethanol
ETU	Energy transfer upconversion
h	Hours
IR	Infrared light
keV	Kilo electron volt
Ln^{3+}	Lanthanide ions
Micrograph	Image taken by microscope
NaF	Sodium fluoride
$NaYF_4$	Sodium yttrium floride
$NaYF_4$:Yb,Er	Sodium yttrium fluoride doped with ytterbium and erbium
$NaYF_4$:Yb,Er@ $NaYF_4$:Nd	Sodium yttrium fluoride doped with ytterbium and erbium and with a shell of sodium yttrium fluoride doped with neodymium
Nd^{3+}	Neodymium ion
NP	Nanoparticle
OAc	Oleic acid
OAm	Oleyl amine
ODAC-TMOS	Dimethyloctadecyl[3-(trimethoxysilyl)propyl]ammonium chloride
ODAOH-TMOS	Dimethyloctadecyl[3-(trimethoxysilyl)propyl]ammonium hydroxide
ORMOSIL	Organic modified silica
PA	Photon avalanche
PTA	Phase transfer agent
RET	Resonant energy transfer
rpm	Rounds per minute
SE	Secondary electrons

SEM	Scanning electron microscope
TEM	Transmission electron microscope
TEOS	Tetraethoxysilane
TFP-TMOS	3,3,3-trifluoropropyltrimethoxysilane
THF	Tetrahydrofuran
TMOS	Trimethoxy(octadecyl)silane
TOABr	Tetraoctylammonium bromide
TOAOH	Tetraoctylammonium hydroxide
UC	Upconversion
UCP	Upconverting particle
Vis	Visible light
XPS	X-ray photon spectroscopy
XRD	X-ray diffraction
Yb^{3+}	Ytterbium ion

INDEX

1. INTRODUCTION

1.1. BACKGROUND AND MOTIVATION FOR MAKING AN OPTICAL CO_2 SENSOR

CO_2 is in the atmosphere, the oceans and in our blood and is through photosynthesis essential to life. High levels of CO_2 indoors cause poor air quality and can even lead to suffocation. In many industries, for instance the food industry, the gas is commonly used and monitored by CO_2 sensors. The sensors have a widespread use, from environmental monitoring to blood samples of patients and general biotechnology. It is the concentration of CO_2 that is of importance. [1, 2]

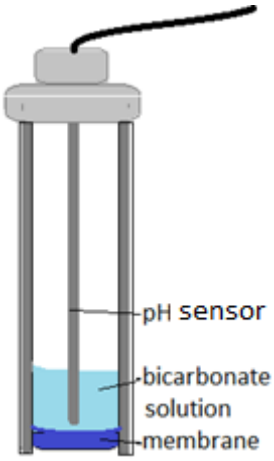

Figure 1 Schematic illustration of the Severinghaus electrode and its respective components

The presence and quantification of CO_2 as a gas is routinely measured by IR spectroscopy or gas chromatography, however both of these techniques require expensive and bulky equipment. When measuring dissolved CO_2, an electronic sensor which is made up of a modified pH sensor with a bicarbonate solution in a gas permeable membrane is used. The device is called a Severinghaus electrode and has been in use for about 50 years but has drawbacks including bulkiness, sensitivity both to electrical interference and to changes in pH induced by gases other than CO_2. [1, 2]

There is a need for quicker and cheaper testing methods [2, 3]. Optical sensors (optodes) are becoming candidates for replacing the Severinghaus electrode. They show good sensitivity towards analytes and are robust, inexpensive and easily miniaturized [1, 2]. The sensing element can be detached from the probe, and so the range of applications is broadened. The current optodes have

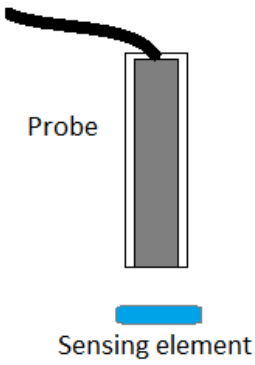

Figure 2 Schematic illustration of an optode

been limited due to the poor photo stability and toxicity of organic complexes and quantum dots that has been used to generate the optical signal of the sensing element [4]. By use of upconverting particles (UCPs) these limitations can be reduced [2, 4], which is why optodes combined with UCPs is an excellent option for producing better CO_2 sensors. The UCPs however are not by themselves sensitive to the analyte, and must therefore be used together with molecules that are often referred to as sensing probes which changes properties in the presence of the analyte [5].

The controlled synthesis of UCPs with regards to morphology and phase has been an ongoing field of research since the beginning of the 2000s [6], and is still an active field of study [7]. Recently much work has been done to produce sub 10-nm particles compatible with biological applications [5]. However, for use in chemical sensors larger particles are more suitable as these show stronger luminescence [8]. A standard method for producing UCPs has not yet been developed. Solvothermal synthesis is compatible with large scale production [9]. With the future goal of commercial production of an optode based on UCPs, the development of a solvothermal method producing UCPs of controlled phase and morphology is to be carried out in this project.

.

1.2. HISTORIC PERSPECTIVE ON UPCONVERTING MATERIALS

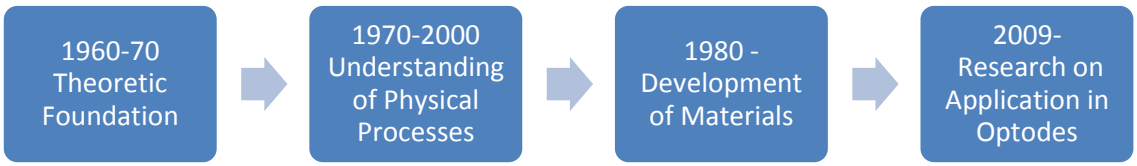

Upconversion (UC) is an optical process where incoming photons of low energy excite a material to emit photons of higher energy [6]. The process will be thoroughly explained in the theory. The concept was suggested theoretically in 1959 by Bloembergen who thought that it was possible to detect and count infrared photons by sequential absorption of an ion in a solid [5, 10]. The concept could not be verified experimentally before the onset of lasers in the 70s. Auzel was a pioneer in the field of UC that gets credited for the discovery of the materials, he also named one of the mechanisms by which the conversion occurs [11].

The first couple of decades the research area of upconversion was mainly within physics [10]. It was found that crystalline materials containing lanthanide ions (Ln^{3+}) showed upconversion. The focus of the research was on understanding the electron transitions and energy transfers that occurred within the upconverting materials. The research resulted in many glasses and other bulk materials that are now used in optical applications such as solid state lasers [12].

With the onset of nanotechnology, 40 years after the publication of Bloembergen's theory, the research on upconverting materials got a boost [6] and the research has moved from physics towards material science, chemistry and applications in biology [5, 13]. Nanoparticles of UC materials have become very popular for use as contrasting agents and bio-labelling because they show higher detection limits than organic complexes and semiconducting nanoparticles [12, 13]. A lot of effort has been put in to producing UC

nanoparticles with controlled morphology and size as this has an impact on the UC efficiency [5].

A material which is now commonly used for UC applications is $NaYF_4$:Yb,Er crystals [5]. It was first reported in 1972 and was synthesized at elevated temperatures in the presence of HF gas [12]. $NaYF_4$ particles on the micrometer scale were produced in 1999, however heat treatment for ten days was necessary to produce the desired hexagonal phase [12]. In 2003 two independent groups synthesised colloidal nanoparticles of upconverting materials and the next year cubic $NaYF_4$:Yb,Er was synthesised [13].

Over the last ten years a huge variation of upconverting particles (UCPs) has been made of varying composition, morphology and size [13], including fluorides and oxides[5, 13], rods, spheres and platelets [12, 14]. It is also possible to have emission of several different colours by varying the lanthanide ions in the material [5]. The most common emitters are Er^{3+}, Tm^{3+} and Ho^{3+} which give out green and red, blue and green colour respectively [5]. Although there is a huge variation of UC materials, several studies are dedicated to $NaYF_4$:Yb,Er due to its outstanding performance [15]. The material has become a standard for groups researching upconversion, and is therefore also the material that will be presented in this work.

Several groups have established that by adding an inactive shell of $NaYF_4$ without Ln^{3+}, the luminescence of the particles is improved [16]. A heat-up method can be used to produce core-shell particles [17, 18]. The method repeats the synthesis of the core particles, while adding the core particles as a precursor for the core-shell structure [18]. This was first used and developed in 2007 and 2008 [18]. By the heat-up method it is also possible to make structures with multiple shells [18].

The reason why a core-shell structure improves the luminescence is that it inhibits quenching of the lanthanide ions (Ln^{3+}) present at the surface of the particle [18, 19]. It is common to coat the particles with a polymer or silica or with a passive shell of the core structure [17]. The newest trend in preparing $NaYF_4$ core-shell particles is to have different Ln^{3+}s in the respective shells [20].

Since 2009 a new application of UC materials has been tried out, namely as signal emitters in optical sensors (optodes). Over the last 30 years professor Wolfbeis and his group at Regensburg University in Germany have been studying and developing optodes. The group has even made a spin-off company making optodes called PreSens[1] and were the first to introduce and prove the concept of using UC materials in a sensing element [8].

There are both dry and wet sensing elements used for CO2 optodes [4], as illustrated in Figure 3. The wet optodes were first engineered in the late 1970's and are based on a dye dissolved in a bicarbonate aqueous solution covered by a gas permeable and ion impermeable membrane [4]. A dry optodes is a dye incorporated in a solid, where the solid usually is a hydrophobic polymer. These could not be made before 1991 when the discovery of phase transfer agents (PTAs) that can make a dye compatible with a hydrophobic environment was done [4].

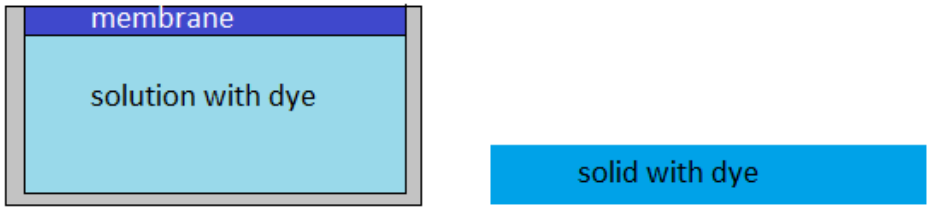

Figure 3 Schematic illustration of wet and dry optode sensing element respectively

Optodes are commercially available from Ocean Optics [2], but optodes applying upconversion are still at an experimental stage. The current research concerning UC materials in optodes is presented in the following chapter.

1PreSens – Precision Sensing. http://www.presens.de/ Accessed 02.04.2015

2Ocean Optics. http://oceanoptics.com/ Accessed 02.04.2015

1.3. PRIOR ART

1.3.1. OPTICAL SENSORS BASED ON UPCONVERTING PARTICLES

Wolfbeis' groups was the first (2009) to use UCPs as "nanolamps" together with a chromophore in a transparent matrix, as illustrated in Figure 4, to produce an optical sensing element for pH [8]. The following years they made similar sensing elements for carbon dioxide [2] and ammonia [21]. The optical sensor for CO_2 was made up of UCPs in a polystyrene film together with the pH indicator bromethyl blue (BTB) and showed sensitivity towards CO_2 concentrations of 0-3 % [2]. The UCPs function as a light source that is filtered through the chromophore that is sensitive to the surrounding environment and hence changes colour dependently [2, 8, 22]. The chromophore and UCPs are not chemically bound, and therefore a change in signal comes from the filtering effect of the chromophore. Another group led by Qin has more recently used the same concept to produce two different sensing elements that are sensitive to lead [23] and potassium [24] ions respectively. A combined hydrogen peroxide and glucose sensor has also been made [25].

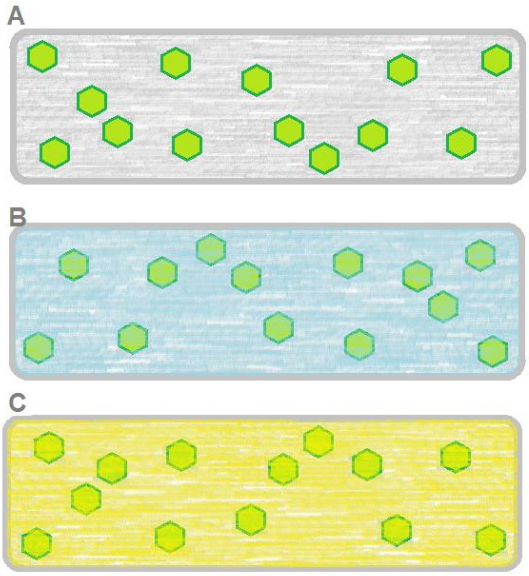

Figure 4 A) Sensing element with green particles acting as "nanolamps". B) and C) variations in filtering by the chromophore, for example induced by changes in pH.

The sensing elements presented by Wolfbeis and Qin were all of a hydrophobic polymer with UCPs of $NaYF_4$:Yb,Er [2, 8, 21, 23, 24]. In our group Magne Kringberg [26] has developed a hydrophobic silica matrix that was also to be used as a sensing element together with quantum dots and BTB or cresol purple (CP) for CO_2 sensing. The $NaYF_4$:Yb,Er of the various sensing elements were synthesized by two different methods, namely solvothermal [8, 23, 24] and co-

precipitation [2, 21]. It is also common to synthesize $NaYF_4$:Yb,Er by a thermal decomposition method [7].

1.3.2. SYNTHESIS METHODS OF UPCONVERTING PARTICLES

The abovementioned synthesis methods recur for producing UCPs [7]. The advantages and disadvantages of the three are summarized in Table 1 [5, 7]. As mentioned in the motivation it is the solvothermal method that will be studied in this paper.

Table 1 Advantages and disadvantages of the three most common synthesis routes for producing upconverting materials.

Method	Advantages	Disadvantages
Thermal decomposition	- uniform and monodisperse particles which are easily dispersed in solution -control of nucleation and growth	-based on fluoride acetates which has toxic gases as by-products -the product must be treated to become hydrophilic
Co-precipitation	- quick method without toxic by-products	-time consuming preparation of precursors - annealing necessary for the product to be of high quality
Solvothermal	-low reaction temperatures -obtainable control over phase, size and shape of the products	- many variables in the reaction that affect the result - inability to monitor the progress of the reaction

There are not many studies dedicated to the development of β-$NaYF_4$ rods by the solvothermal method. Following is a summary of what has been done.

Zhang et al. [14, 27] did a thorough study on the effects of the concentration of Y^{3+} and F^- and NaOH on the morphology of the samples, and reported how temperature and time influence the phase transition from α- to β-phase of $NaYF_4$ [27]. The group has also produced ordered arrays of hexagonal tubes with lengths of about 500 nm, and found that these grew in the [0001] direction. With increased concentrations of NaF the tubes grew into rods and excess NaF was present in the product. When the amount of the surfactant oleic acid (OAc) was increased the particles formed were hexagonal platelets. [14]

Recently Ding et al. [28] also investigated the effects of reaction time of the solvothermal synthesis on the produced $NaYF_4$ as explained in section 2.3.1. The group further investigated how changing the sodium precursors and altering pH, affected the product. It was found that an increase of pH from 7 to 11 changed the morphology of the rods to shorter rods, tubes and even torus shaped particles. The group concludes that the pH dependency of the shape arises from adsorption ability of the surfactant on the surfaces of the particle, and that OAc is weaker bound to the (0001) planes of the crystal. The different sodium precursors were $NaBF_4$, NaF and NH_4F, all of which produced rods, however with varying sizes and aspect ratios. [28]

Guo et al. [29] found that a mixture of water, ethanol, glycol and OAc was optimal for producing hexagonal nanorods compared to any of the solvents alone [29]. The groups of Zhang and Ding both used OAc as surfactants, as will be done in this project, other groups have used cetyltrimethylammonium bromide, ethylenediaminetetraacetic acid and sodium poly(4-styrenesulfonate) [12, 30-32]. Gao et al. [30] has investigated the luminescent properties of $NaYF_4$:Yb,Er when changing Yb^{3+} and Er^{3+} concentrations. Jiao et al. [31] investigated varying the concentration of the surfactant as well as the effect of pH on the morphology an luminescence of the product. Wang et al. [32] studied the morphological effects of changing the concentration of the surfactant as well as varying pH and the fluoride source. Lin et al. [33] simply used water as solvent without the presence of a surfactant and studied variations of pH and time. The obtained product

at pH 1.5 was YF_3 and the phase transition from α- to β-phase of $NaYF_4$ was observed at higher values of pH and longer reaction times.

Liu et al. [34] studied $NaLuF_4$ doped with various combinations of Ln^{3+}, and in particular how the ratio of sodium fluoride to lanthanide precursors affected the morphology and luminescent properties of the product. The group found that a low ratio lead to the formation of α-$NaYF_4$ and that by increasing the amount of NaF there was a transition through mixed phases and eventually pure β-$NaYF_4$, however with excess NaF still present in the product as found previously by Zhang et al.. The products produced with a larger amount of NaF also showed stronger luminescence [34].

1.3.3. ND^{3+} SENSITIZED UPCONVERTING CORE-SHELL PARTICLES

As mentioned in section 1.2, core-shell structures may be used to incorporate several different Ln^{3+}s in the same material. This makes it possible to separate the ions spatially in the matrix of the host material, avoiding non-radiative relaxation between the ions. Zhong et. al [20] term the various methods of incorporating Nd^{3+} together with Yb^{3+} and Er^{3+} in a core-shell structure based on $NaYF_4$ for 1st, 2nd and 3rd generation core-shell UCPs [15, 20, 35]. An overview of the materials is given in Table 2 and the differences are explained further in the theory section 2.2. All three generations have been synthesized by applying the thermal decomposition method [15, 20, 35], opposed to what will be done in this project where the solvothermal synthesis will be applied.

Table 2 Overview of the various generations of core-shell particles incorporating Nd^{3+} together with Yb^{3+} and Er^{3+}. To the left of @ is the abbreviated chemical formula of the core. @ indicates a core-shell structure with the abbreviated chemical formula of the shell to the right.

Generation	Notation
1st	$NaYF_4$:Nd,Yb,Er@$NaYF_4$
2nd	$NaYF_4$:Nd,Yb,Er@$NaYF_4$:Nd
3rd	$NaYF_4$:Yb,Er@$NaYF_4$:Yb@$NaNdF_4$:Yb

1.4. AIMS AND OUTLINE OF THE THESIS

1.4.1. AIMS

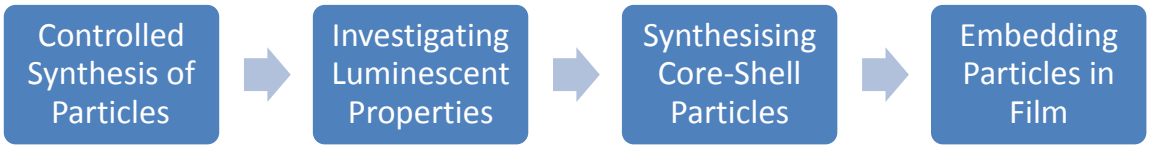

The ultimate goal of the project was to produce a sensing film suitable for a CO_2 optode. By introducing the upconverting particles (UCPs) in a hydrophobic silica sol-gel matrix together with the chromophore bromethyl blue (BTB); it should be possible to detect the change of CO_2 concentration in solution by measuring the intensity of the emitted light. Core-shell UCPs with neodymium in the shell, would make it possible to avoid problems of heating previously encountered for excitation at 980 nm. UCPs have so far only been imbedded in polymer matrices and not silica based films for sensing, as will be described in this thesis. This work is mainly based on the article "pH Sensor based on Upconverting Luminescent Lanthanide Rods" by Sun et al. [8].

UCPs have not previously been synthesized or characterized at the University of Oslo. For this reason the most important aim of the project has been to find and develop a simple synthesis strategy for UCPs, as well as to look at which characterization methods are suitable for the sample. Solvothermal synthesis is a common method for producing highly crystalline powders, and was to be applied to produce rods of β-NaYF4 which is an excellent host material for UC. The effect on the physical and optical properties of the product by varying synthesis parameters such as temperature and the addition of surfactants were to be studied.

To study and understand the various outcomes in morphology, composition, size and luminescent properties, the particles were to be examined by x-ray diffraction (XRD), scanning and transmission electron microscopy (SEM and TEM), x-ray photon spectroscopy (XPS) and photo spectrometry. Rods with core-shell structures that can be excited by 800 nm laser have, to the best of our knowledge, never been synthesized. Therefore to combine possibility of adding a shell to the rods and upconversion at 800 nm was also to be investigated.

1.4.2. OUTLINE

In the following chapter, the physical property of upconversion is explained as well as the necessary features of the materials showing this property. Then the concept of the CO_2 optode is explained before an outline of the theory behind the synthesis methods and abovementioned characterization techniques is given.

A detailed section describing the experimental procedures of both synthesis and characterization follows the presentation of the necessary theory, and the results and discussion chapter is set up in a similar order as that of the experimental. First the results connected to the particles are shown and discussed. Second the results of the optical properties of the samples are given before a brief section on the sensing element is presented. Finally there is a conclusion and presentation of possible further work and future challenges of the development of core-shell β-$NaYF_4$ and the field of UC.

2. THEORY

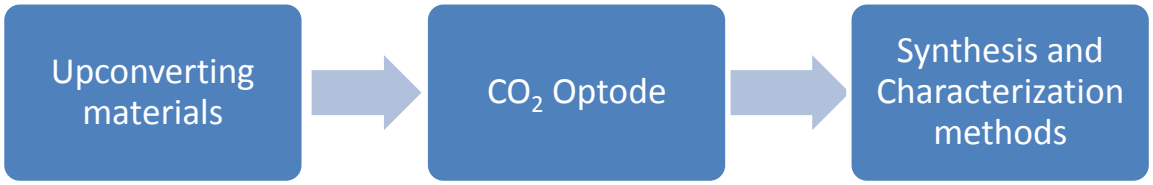

2.1. UPCONVERSION MATERIALS AND $NAYF_4$-CRYSTALS

Upconversion (UC) materials can be classified as functional materials as opposed to construction materials. Functional materials are characterized by intrinsic properties such as electric, magnetic and optical properties that are often also susceptible to the size of the material. The functional properties are in particular dependent in the electron configurations of the material, and features such as band gap and electron transitions needs to be understood. This is opposed to construction materials, which are categorized according to mechanical properties such as tensile strength and ductility.

The most common UC materials [6] have sensitizer and activator ions embedded in a host matrix, also simply referred to as the host. The sensitizer and activator are the ions responsible for the energy conversion of the light. The host is a crystalline material where each chemical element is placed in a three dimensional grid referred to as a lattice. The host spatially separates the ions to optimize energy transfer between them. The UC process requires successive absorption of photons, and so a prerequisite for the material is intermediate energy levels of the activator ions.

The functional property of UC materials is the ability to convert low energy light to light of higher energy by multiple phonon absorption, hence the term UC. There are three main models for explaining UC which is an anti-Stokes mechanism [11]. Each model is connected to the ion doping of the excited material [6]. An illustration of two of the

processes is shown below in Figure 5 and the descriptions of all three are taken from "Upconverting Nanoparticles" [6].

Excited state absorption (ESA) happens by a successive absorption of photons by a single ion. The first photon excites the ion to an intermediate excited state and then a second photon further excites the ion to a higher excited state from which emission occurs. *Photon avalanche* (PA) is an interaction between more ions, where one ion is excited by photons to a higher excited state. Then the ion relaxes by exciting a neighbouring ion so that they are both in an intermediate excited state. Now these two ions will be excited into higher excited energy states, further exciting neighbouring ions. This continues until an avalanche of emission occurs and the ions are relaxed to the ground energy state.

The UC materials of PA–type have a low doping concentration whereas materials which show *energy transfer upconversion* (ETU) have a higher level of doping. ETU is the most common mechanism for UC and the one presumed to occur in the material presented in this paper. The ion that first absorbs the photons is called a sensitizer and will have a band gap matching that of the incoming light. Then there is an energy transfer to another

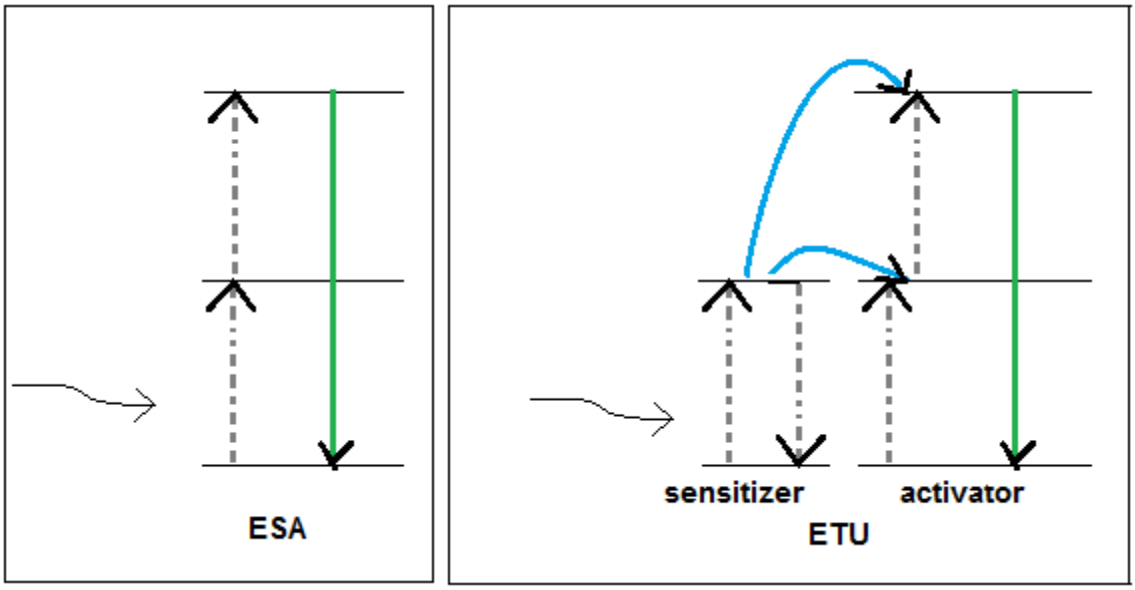

Figure 5 Schematic illustration of the energy excitation and relaxation (dotted lines), transfer (curved blue lines) and emission (straight green lines) of the ESA and ETU mechanisms of upconversion. The sensitizer absorbs and the activator emits light.

ion, called the activator which has energy levels compatible with that of the sensitizer. The activator is excited to an intermediate excited state, then further to a higher excited state by a second photon through energy transfer by the sensitizer, and then emits light as the material relaxes to the ground state.

The activator and sensitizer in the UC material are lanthanide ions (Ln^{3+}) [11]. The Ln^{3+} all show similar properties due to the similar electron configuration, $[Xe]4f^n5d^16s^2$, where n depends on the specific ion [11]. The energy levels of the ions are evenly separated and are often referred to as having a ladder-like configuration. This configuration fulfils the criteria of intermediate energy levels necessary for the UC process [11]. Except for La^{3+} and Lu^{3+} which lack unpaired 4f electrons, the Ln^{3+}s give out emission from 4f-4f transitions [11]. The f-f transitions are forbidden and therefore unlikely to occur, so the excited states have prolonged lifetimes [3] making the successive absorption of the photons more likely.

The Ln^{3+} most often encountered in UC materials are Yb^{3+}, Er^{3+} ,Ho^{3+} and Tm^{3+}[11]. Yb^{3+} is used as sensitizer because of its few energy levels as illustrated to the left in Figure 6. This makes the chances of cross-relaxation with the activator less likely. Cross-relaxation is an energy transfer process where the activator ion transfers energy back to the sensitizer, instead of emitting light [10]. Er^{3+} as well as Ho^{3+} and Tm^{3+} are good activators for UC because their energy levels have the ladder-like configuration and are compatible with the energy gap of Yb^{3+} [11].

A good host has low phonon energies which leads to longer lifetimes of the excited states and reduces non-radiative emission [6]. Fluorides and oxides are both common UC hosts but oxides have a much higher phonon energy and are therefore not as good as fluorides [6]. Concerning the host, impurities in the lattice will affect the UC efficiency [11]. The material should therefore be based on Na^+, Ca^{2+} and Y^{3+} cations which have similar ionic radii as the Ln^{3+} because this facilitates doping of the material, without causing a mismatch in the lattice and hence strain to the structure [11].

The excitation of Er^{3+} by Yb^{3+} can be explained by the previously mentioned ETU mechanism and the following Jablonski diagram [3]. The levels show the electronic energy levels of the ions and the arrows illustrate excitation, transfer and relaxation of the electrons between the levels.

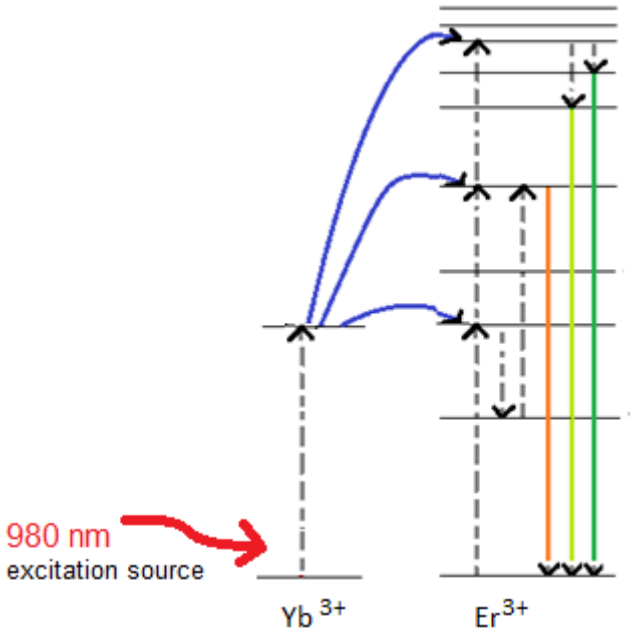

Figure 6 Jablonski diagram of the excitation successive excitation of Yb^{3+} and Er^{3+} by IR laser. Curved lines represent energy transfer, dashed lines are excitation or relaxation of the electrons and straight lines show emission.

The dashed grey arrows pointing directly upwards illustrate excitation of the energy levels whereas the downward pointing dashed arrows illustrate relaxation. Yb^{3+} is excited by an infrared (IR) laser as shown by the red arrow. Then by energy transfer (curved blue arrows) Yb^{3+} successively excites Er^{3+} in ladder like steps through an intermediate excited state until emission occurs. The figure above also shows which energy levels are included in the excitation and emission of the varying wavelengths. The red emission is at 630-680 nm and the green at 510-570 nm [14].

A material that fulfils the abovementioned criteria and which is one of the most common UC materials today are sodium yttrium fluoride doped with ytterbium and erbium ($NaYF_4$:Yb,Er), where Yb^{3+} is the sensitizer and Er^{3+} the activator. In the $NaYF_4$ material there is a substitution of Y^{3+} by Yb^{3+} and Er^{3+}. Usually Yb^{3+} and Er^{3+} make up 18 and 2 atomic percent of the material respectively, which gives the chemical formula of $NaY_{0.8}Yb_{0.18}Er_{0.02}F_4$ [6]. This composition has been found to give the maximum absorption by Yb^{3+} and emission of Er^{3+}, without causing cross-relaxation [36].

$NaYF_4$ has one kinetically and one thermodynamically stable phase, which is of cubic and hexagonal structure respectively [6]. The cubic phase is often also referred to as α-$NaYF_4$ and the hexagonal one as β-$NaYF_4$. The hexagonal phase is known to show better UC efficiency than the cubic [6], and this property is assigned to the different placements of the Ln^{3+} in the lattice. Although β-$NaYF_4$ is thermodynamically more stable, it is unfortunately the most difficult phase to synthesise [7].

In addition to the phase, the morphology of the host crystal also has an effect on the UC efficiency. Rods show better UC than spheres, disks and tubes [8, 14]. This might be linked to the surface area-to-volume ratio of the particles, and can explain why larger particles show better UC efficiency. A smaller surface area-to-volume ratio, means less sensitizer and activator ions on the surface when these are evenly distributed in the material. The ions are prone to quenching on the surface, and so if there are fewer ions on the surface, the probability of quenching is less. The quenching, or deactivation of the ions can be caused by surface defects, surfactants on the surface of the particles and other molecules in the solvent surrounding the particles [19].

2.2. CHANGING EXCITATION WAVELENGTH

A challenge in applications relying on $NaYF_4$:Yb,Er is the excitation wavelength at 980 nm. This corresponds to one of the highest absorbance peaks of water, Figure 7 [20, 35], which means that for measurements using the material in any medium containing water, much of the excitation will be absorbed at a very short path length. It also leads to heating of the sample [15, 20, 35].

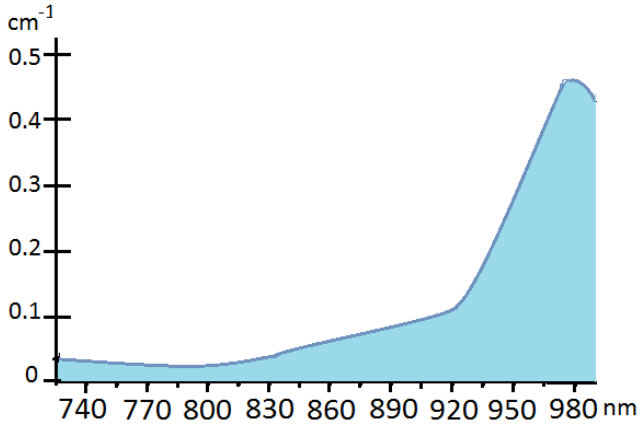

Figure 7 The absorbance of light of IR light in water, there is a local minimum around 800 nm, and at 980 nm the absorbance is quite high.

Heating is of concern for CO_2 sensors because they are sensitive to changes in temperature as will be explained in the theory of optodes in section 2.3. To overcome this limitation, it is possible to exchange Yb^{3+} with Nd^{3+} in the material, $NaYF_4$:Nd,Er, resulting in an excitation wavelength of 800 nm which corresponds to a local minimum for absorption of light in water [15, 20, 35] .

Nd^{3+} does not have the simple energy diagram such as Yb^{3+}, see Figure 8, which makes it exposed to cross-relaxation, resulting in poor emissions. Fortunately it is possible to combine the use of Nd^{3+} and Yb^{3+} by separating the ions in a core-shell structure [35]. Then Nd^{3+} acts as sensitizer, whereas Yb^{3+} now becomes an energy bridging ion between Nd^{3+} and Er^{3+} [35]. This is illustrated in the following Jablonski diagram [35]. Although Nd^{3+} absorbs the incoming light, Yb^{3+} must still be present in order to excite Er^{3+} and have successful light emission from the material [35].

Core-shell particles previously synthesized containing Yb^{3+}, Er^{3+} and Nd^{3+} are referred to as 1^{st} - 3^{rd} generation particles. 1^{st} generation particles have all of the lanthanides together in the core with an inactive shell of $NaYF_4$ [35]. The doping level of Nd^{3+} must be held below 1 atomic percent to omit cross relaxation between Nd^{3+} and Er^{3+} [35]. 2^{nd} generation particles [15] have the same core as the 1^{st} generation. However, instead of an un-doped shell, there is 20 atomic percent of Nd^{3+} in the shell which increases the absorption efficiency of the incoming light [15]. The 3^{rd} generation particles

have Yb^{3+} and Er^{3+} in the core completely separated from Nd^{3+}, which is only in the outermost shell [20]. Another change from the former generations is that the structure also has an intermediate shell [20]. The resulting sandwich structure consists of $NaYF_4$ doped with Yb^{3+} and Er^{3+} as the core, Yb^{3+} in the middle shell and $NaNdF_4$ doped with Yb^{3+} as the outer shell. In the outer shell an atomic percent of 90 of Nd^{3+} is achieved increasing the particles ability to absorb the incoming light and thus increase the UC efficiency further[15, 20]. Yb^{3+} is kept in all of the layers to ensure energy transfer between the ions. Thermal decomposition combined with the heat-up method has been used in the synthesis of all of these variations, resulting in spherical particles [15, 20, 35].

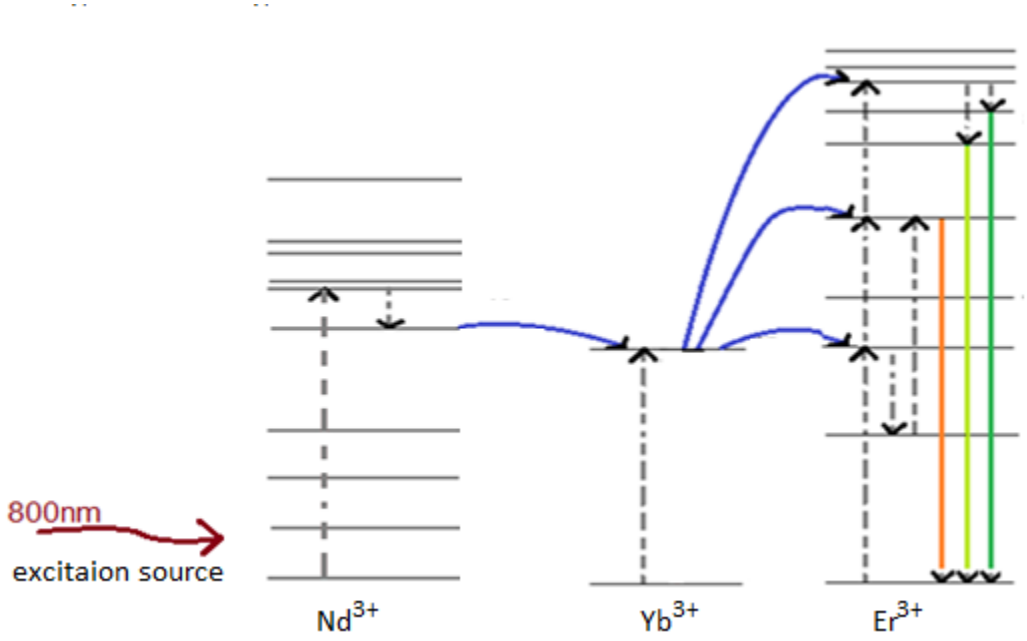

Figure 8 Jablonski diagram of the excitation successive excitation of Nd $^{3+}$, Yb^{3+} and Er^{3+} by IR laser. Curved lines represent energy transfer, dashed lines are excitation or relaxation of the electrons and straight lines show emission.

2.3.OPTICAL SENSORS

An optical sensor, or optode, is an electronic device that reacts to stimuli by changing its optical properties. These properties include for instance the refraction index, absorption spectrum, luminescence intensity and several others. The optical sensor described in this thesis is based on a change in luminescence intensity in the presence of CO_2 gas.

CO_2 sensors are, as previously mentioned in the motivation, based on changes in pH. A CO_2 optodes will therefore have a chromophore (dye) that changes optical properties with changing pH of the system. In dry sensing elements, as mentioned in section 1.2, it is necessary to use phase transfer agents (PTAs) to make the dye compatible with a hydrophobic environment by forming an ion pair with the dye [4]. The dry sensor elements are usually made up of an ion-pair, an organic base and either organic polymers or organically modified silica (ORMOSIL) [1]. The ion-pair, will always have some crystal water associated with it. CO_2 gas diffusing into the sensor matrix will therefore be able react with this crystal water to form carbonic acid, the carbonic acid then protonates the dye changing its colour. It is important that the dye is in its deprotonated form in the matrix, hence the addition of organic base [26]. For CO_2 the pK_a of the dye should be between 7.5 and 9 [4]. These sensors can be used in both dry and humid gases as well as in aqueous solution [1].

Equation 1 [1] illustrates the equilibrium reaction of CO_2 dissolved in water with the presence of a dye-PTA ion pair, here presented as (Q^+D^-) :

$$Q^+D^- \cdot xH_2O + CO_2 \leftrightharpoons Q^+HCO_3^- + HD \cdot (x-1)H_2O \quad (eq.1)$$

The pK_a value of BTB is within the range mentioned above and the changes in colour due to changes in pH. Furthermore its absorption spectrum overlaps with the emission spectrum of $NaYF_4$:Yb,Er creating an inner filter effect [8].

Given equilibrium constant of equation 1, α', it is possible to relate the initial absorbance of the colour dye, A_0, and the absorbance when CO_2 is present, A_D, to the partial pressure of CO_2, P_{CO2}, through the following equation [1]:

$$R_C = \frac{A_0 - A_D}{A_D} = \alpha' P_{CO_2} \qquad (eq. 2)$$

Because it is the signal of the UCP that will be detected in the optical sensor, equation 3 is the one to be used to determine the CO_2 concentration. Given a luminescent signal, the experiments are based on luminescent intensity and not absorbance and hence the equation becomes [1]:

$$R_L = \frac{I_0 - I_D}{I_D} = \alpha' P_{CO_2} \qquad (eq. 3)$$

A huge drawback for all CO_2 sensors is that the equilibrium of equation 1 is temperature sensitive, making the measurements highly sensitive to temperature as well [1]. This is also true for the Severinghaus electrode mentioned in the motivation [1].

THEORY OF SYNTHESIS METHODS AND CHARACTERISATION INSTRUMENTS

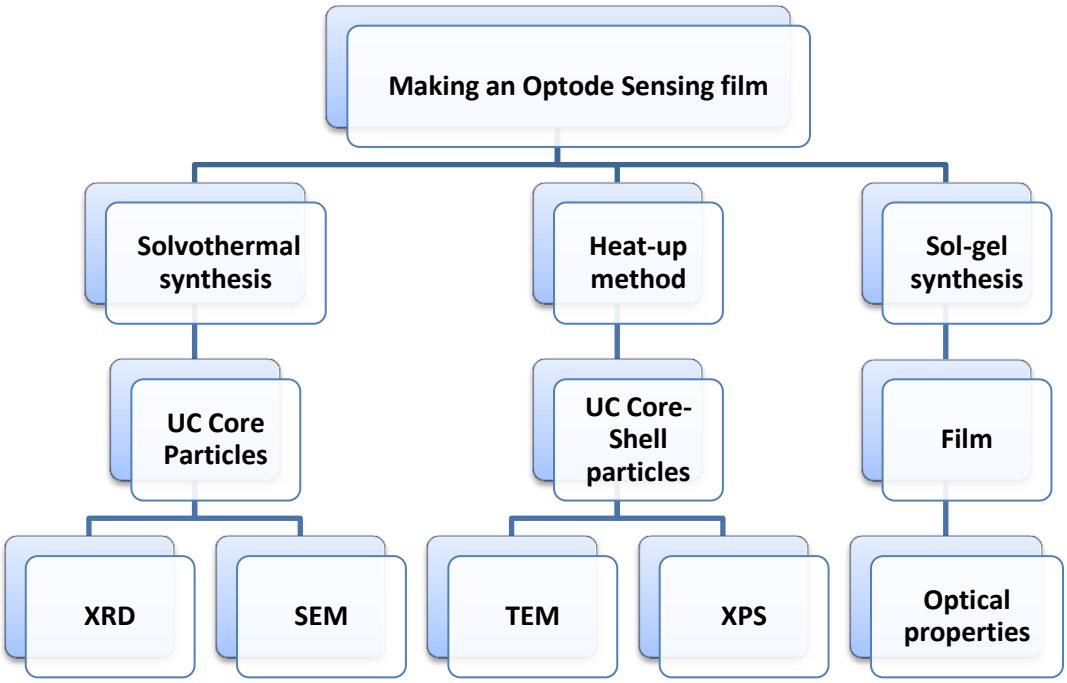

This chapter will outline the theory behind the equipment and procedures used to synthesize and characterize the particles. An overview of the synthesis methods, the products and characterization methods are given in the figure above. The theory of the solvothermal and sol-gel synthesis methods are outlined to give an introduction before the experimental details. A brief theory of the various characterization methods is presented to give a foundation by which to explain the results of the thesis.

2.3.1. SOLVOTHERMAL SYNTHESIS

For this project we chose to work with the solvothermal method of synthesizing upconverting $NaYF_4$:Yb,Er particles because of its several advantages, as given in Table 1. It is a straight forward method that forms highly crystalline products at relatively low temperatures without harmful by-products. A solvothermal reaction is one that happens in a solution at elevated pressure and temperature in a closed vessel [9]. Usually the

parameters are close to the critical point of the liquid to increase solubility and reactivity of the reactants [37].

An experiment at the laboratory scale has the reactants mixed together, then transferred to a Teflon liner which in turn is placed in a sealed autoclave. The use of an autoclave is necessary because of the elevated temperatures and pressure during the reaction. For this reason an awareness of the level of filling of the liner is important so that the conditions will not be so extreme as to explode the autoclave [9]. One disadvantages that is frequently mentioned concerning the method is the inability to observe the reaction as it proceeds [37]. However, it is fairly simple to prepare several autoclaves at once and simply retrieve these from the oven to investigate the course of the reaction.

From their investigation on the effect of reaction temperature and time, Zhang et al. [14] propose that the solvothermal synthesis of β-$NaYF_4$ happens through dissolution-reconstruction. This is backed up by Ding et al. [28] who also has SEM images supporting the theory. Figure 9 is an illustration of the proposed reaction mechanism. When mixing the reactants, a microemulsion is formed containing reverse micelles. The reverse micelles are made up of the surfactant molecules coordinated with Ln^{3+} ready to react with the fluoride ions also present in the microemulsion (A). Then upon heating the reverse micelles function as confined reactors. At low temperatures α- $NaYF_4$ is formed (C), and at higher temperatures β-$NaYF_4$ is observed. The group further believes that there is dissolution of α- $NaYF_4$ at higher temperatures or longer reaction times, that leads to the growth of β-$NaYF_4$ crystals and that this can be partly explained by Ostwald ripening (D-E) [14, 28]. The difference in solubility causing the Ostwald ripening effect however, is not present for particles larger than 5 nm in diameter [9].

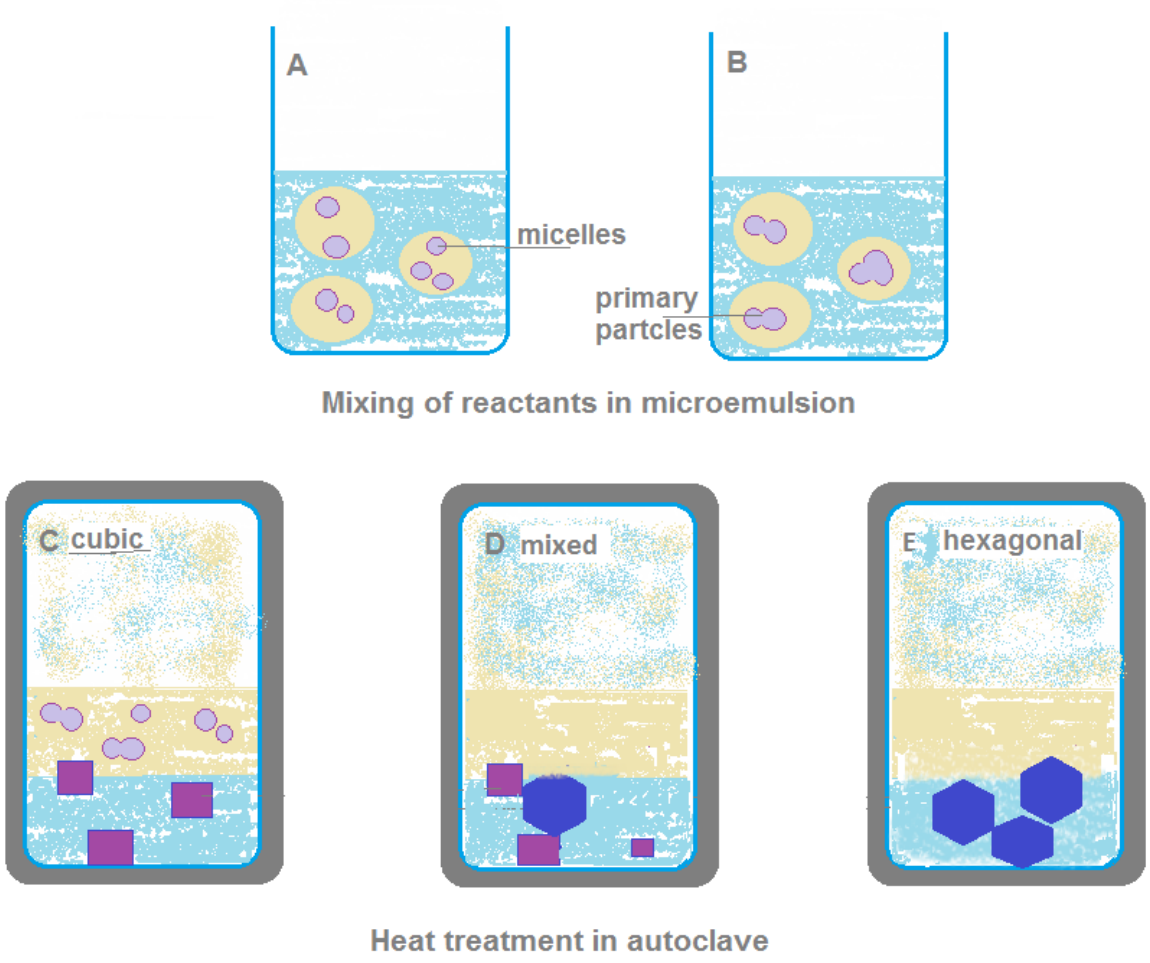

Figure 9 Schematic illustration of the proposed dissolution-reconstruction process of the course of the reaction happening in the solvothermal synthesis method. First the reactants are mixed (A,B) forming a microemulsion of micelles and primary particles. Then the products are formed (C - E) with hexagonal particles forming at higher temperatures and longer reaction times.

2.3.2. THE SOL-GEL PROCESS

The sol-gel process [9] is commonly used to make silica gels. In principle the mixture of reactants first forms colloidal particles and is called a sol. These particles bond to form an amorphous network in the solution. When this network spans the whole volume of the solution it is called a gel. For silica materials this process happens through condensation and gelation as illustrated in Figure 10.

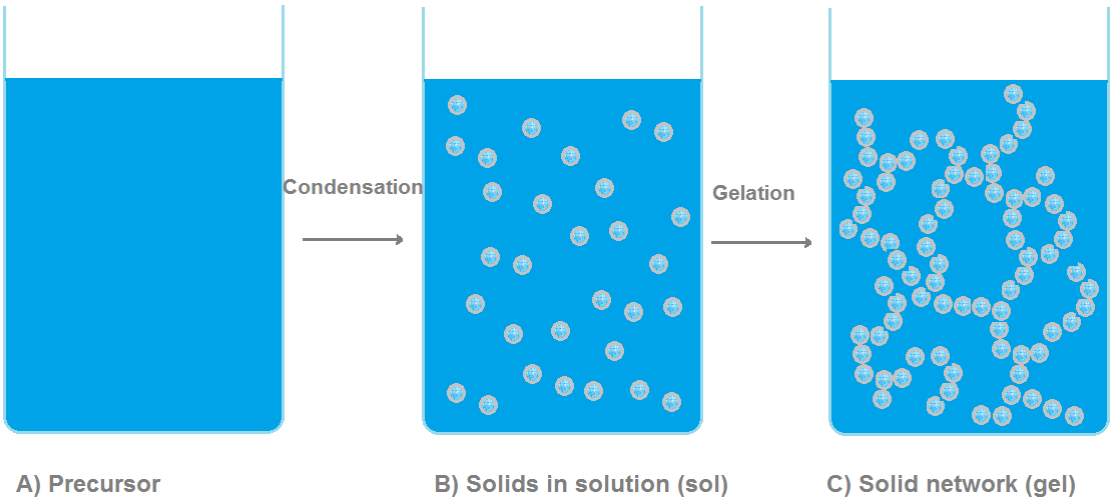

Figure 10 Schematic illustration of the sol-gel process. Starting with the precursors (A) that undergo condensation to form the sol (B) which then further reacts to form a solid network called a gel (C)

Condensation is the description of alkoxides and silanols combining to form siloxanes with alcohols and water as by-products. The most common starting materials are tertramethoxysilane (TMOS) and tetraethoxysilane (TEOS) and the reaction uses either an acid or base as catalyst. By referring to equation X the process might seem trivial, however the condensation reactions are all equilibrium reactions and therefore several outcomes are possible during the process.

$$Si(OR)_4 + 2H_2O \rightarrow SiO_2 + 4ROH \quad (eq.4)$$

The final product of the condensation reactions is the sol. Whether it remains a sol or continues through gelation to form a gel depends on the stability of the sol. That is because the colloidal particles must aggregate to form the gel. By definition the transition from sol to gel is complete when you can turn the beaker upside down and no liquid is spilled. The time of the transition greatly depends on the catalyst used. Without a catalyst it could be more than tenfold that obtained with HCl as catalyst which is about 96 hours. Even after the sol has become a gel the gel can change properties. That is because there are still open bonds that can react. The process is called aging and makes the gel stiffer. Further the gel is prone to drying which causes the gel to shrink and possibly even collapse.

2.3.3. X-RAY DIFFRACTION

X-ray diffraction (XRD) is the most common technique for structure determination of crystals [38]. Because the wavelength of the x-ray beam corresponds to the distance between the crystal planes, constructive and destructive interference occurs as the beam is diffracted by the planes [38]. This gives a diffraction pattern. Bragg's equation is used to identify the crystalline phases in a material [39]:

$$n\lambda = 2d\sin(\theta) \qquad (eq.5)$$

n is a whole number, λ the wavelength of the X-ray beam, d the distance between the planes within the crystal and θ the angle between the beam and the plane.

When Bragg's law is fulfilled the equation can be used to calculate the distances between the planes[39]. Then by further calculations the lattice parameters of the crystal can be obtained. A diffraction pattern, such as the one in Figure 11, is made up by the intensity of the signal at each 2θ value and is unique to a material because each plane in the crystal has a given intensity at a given angle[39].

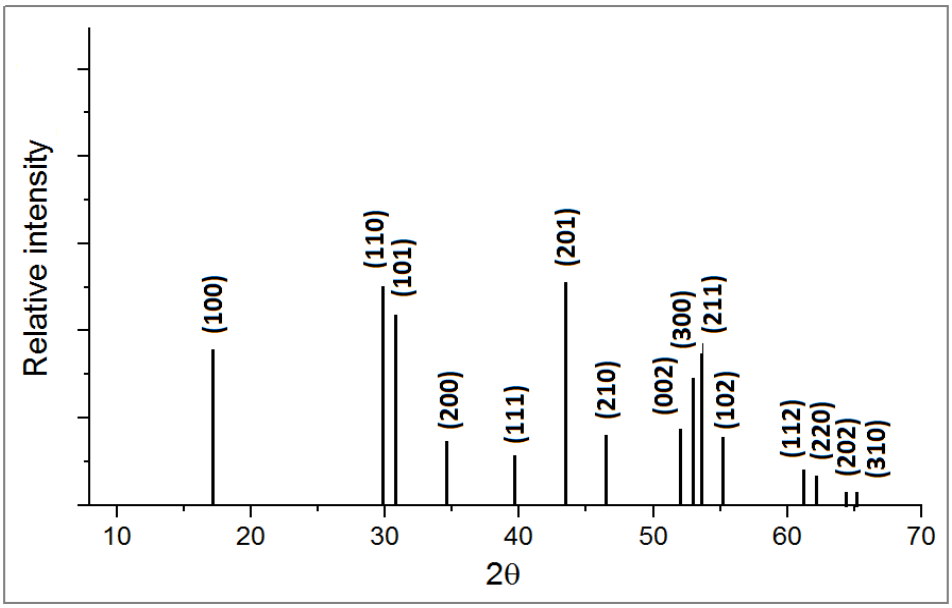

Figure 11 Diffraction pattern as the one calculated for β-$NaYF_4$:Yb,Er # 00-028-1192 in the PDF crystallographic database with the planes indicated in brackets.

From the diffraction pattern of a sample it is possible to get information about the materials and their crystallographic phases by the characteristic positions of the peaks identified by comparison with a diffraction standard catalogued in a database [39]. The intensity of the peaks can also give information about the shape of the particles [14].

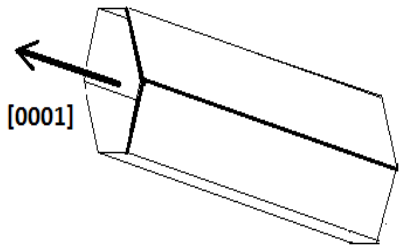

Figure 12 The hexagonal structure of a β-NaYF4 rod, with the arrow indicating the anisotropic growth along [0001] direction

For instance for particles of β-$NaYF_4$ the shape of the particles are often hexagonal rods [40]. With anisotropic growth in the [0001] direction, as illustrated in Figure 12, the rods give a higher than calculated relative intensity of the (100) peak. Finally the width of the peaks at half-height can be used to determine the size of the particles. Wider peaks indicate smaller particles [trenger ref].

2.3.4. ELECTRON MICROSCOPY

Electron microscopes are used to look at the morphology and composition of materials and are in some ways like regular light microscopes [38, 39]. The sample is illuminated and either the transmitted or the reflected signal is detected. The difference being that the source is an electron beam which gives a higher resolution than light and that this requires vacuum [38, 39]. Scanning electron microscopes (SEM) apply the electron beam to scan over the sample and electrons are scattered to a detector on the same side of the sample, and transmission electron microscopes (TEM) detect the electrons that are transmitted through the sample [39]. For this reason the electron current is different for the two instruments. For TEM it is set between 100 to 400 keV whereas for SEM it is only necessary with currents of 3-30 keV [39]. Modern versions of the two microscopes also have scanning transmission electron microscope (STEM) modes. This allows both the electron beam to scan the sample and the signal to be detected after transmission through the sample [39].

2.3.4.A. SCANNING ELECTRON MICROSCOPY

The SEM detects three different signals: Back scattered electrons (BSE) tells about the atomic number or weight of the phases because the BSE have been scattered by the atomic cores[39]. Secondary electrons (SE) show the topology of the sample as these are scattered by the electron clouds around the atoms[39]. Finally X-rays give energy dispersive spectra (EDS) with information about the atomic and weight percentages of the different elements present in the sample [39]. It is also possible to do EDS by TEM when applying the STEM mode [39].

2.3.4.B. TRANSMISSION ELECTRON MICROSCOPY

By TEM [39] the morphology and composition of the sample is investigated by looking at the mass-thickness contrast or diffraction contrast. Mass-thickness contrast is self-explanatory as the contrast of the image depends on the mass of the elements in the sample and the thickness of the sample . That is because the electrons are deflected as they travel through the sample and heavier elements scatter electrons more, giving rise to a higher contrast. Diffraction contrast comes from the lattice planes of the crystalline sample that scatters the electrons in various directions.

From TEM it is also possible to obtain diffraction patterns as the electrons follows Bragg's law given the wave-particle duality of electrons. From the diffraction patterns it is possible to obtain the d-values of the crystal lattice by equation 6 [39]:

$$d = \frac{2\lambda L}{2R} \qquad (eq.6)$$

Where d is the d-spacing of the lattice, λ the wavelength of the electron beam, L the camera length of the instrument and R the radius of a ring in the diffraction pattern [39].

2.3.5. X-RAY PHOTOELECTRON SPECTROSCOPY

X-ray photoelectron spectroscopy (XPS) [38] is used for chemical analysis of the surface of materials. The technique looks at the characteristic energy of the electrons that are emitted from the solid when it absorbs x-ray emission as illustrated in Figure 13.

An incident photon of sufficient energy may knock out an inner shell electron of an element (Figure 13B). This is shown in the illustration below. The electron is then ejected as a photon with a specific kinetic energy, E_K (Figure 13C). By measuring E_K it is possible to calculate the binding energy, E_B, of the inner shell electron by the following equation [38]:

$$E_B = h\nu - E_K - \phi \qquad (eq.7)$$

where hν is the energy of the incident photon and ø the work function of the material, and are both given values.

Each value of E_B is characteristic for the element, and hence the method can be used for element identification in a sample. An XPS spectrum shows the electron intensity versus E_B of the electrons ejected by the sample. By comparing lists of E_B values to the obtained spectrum the peaks of the spectrum can identified as belonging to certain elements. The position of the peaks may also be affected by the instrument and sample surface; therefore internal standards are often used. [38]

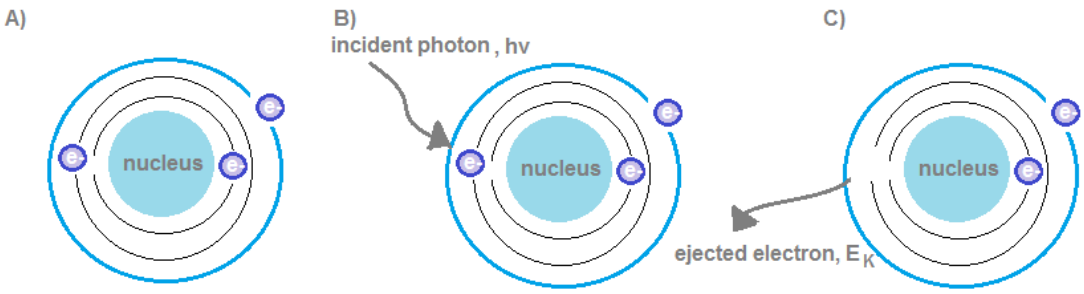

Figure 13 Illustration of A) atom B) atom bout to be excited by a photon C) atom where an electron has just been ejected.

2.3.6. PHOTOLUMINESCENCE SPECTROSCOPY

For optical measurements of UC materials, it is necessary to have and excitation source and a mode of detection. The easiest is to have a probe at which both the excitation is emitted and the signal detected. The excitation source must be one that is compatible with the sensitizer in the UC material as explained in previous theory 2.1. For $NaYF_4$:Yb,Er the obtained spectrum will look like Figure 14 [27]. The detection of the signal is done through a fiber cable that is connected to a spectrometer. The spectrometer functions as a transducer which changes the optical signal from the sample to an electronic signal that can be read by the computer. The technique is limited by the detection limit of the probe, as well as the detection interval of the spectrometer. For the particular setup of Figure 15 saturation of the excitation signal due to reflection of the sample plate may also be a problem.

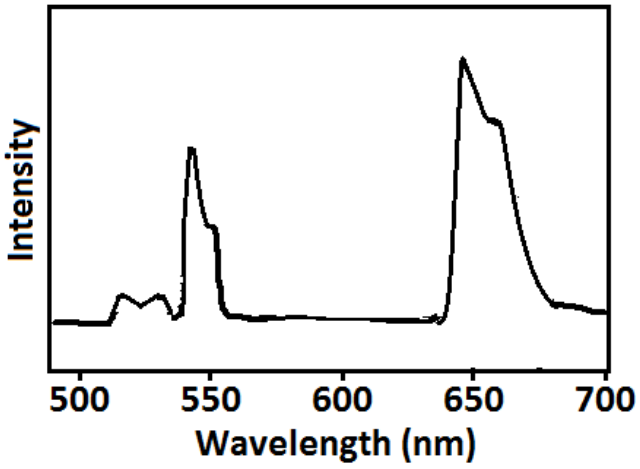

Figure 14 An illustration of the characteristic peaks of a luminescent spectrum of $NaYF_4$:Yb,Er by excitation of 978 nm IR excitation

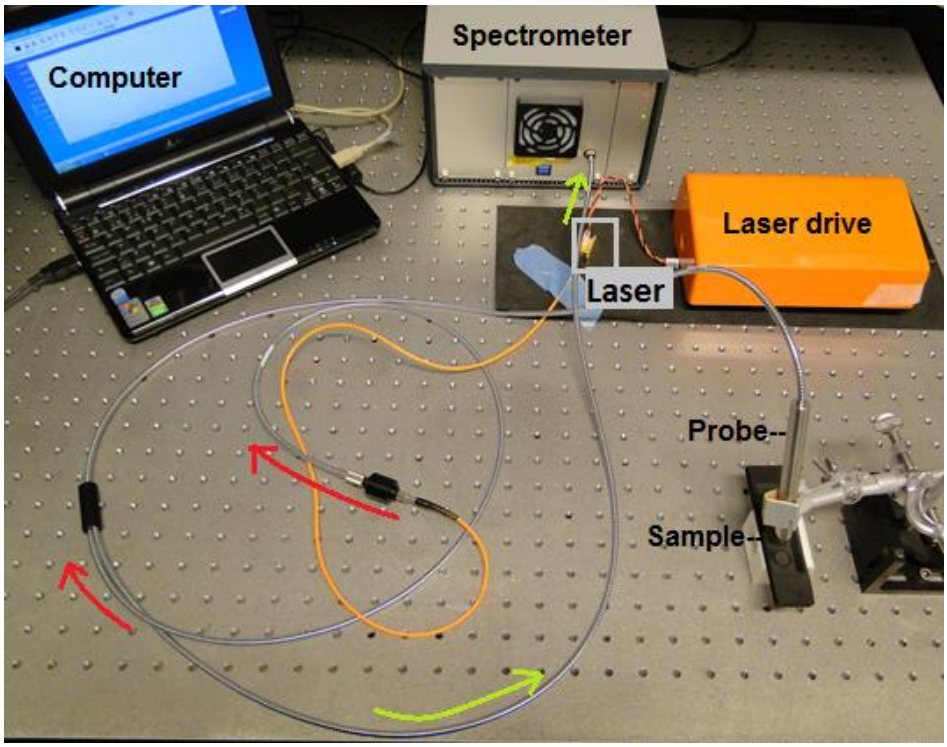

Figure 15 Overview of setup for the optical measurements. The red arrows indicate direction of the laser light. The green arrows indicate the direction of the signal from the probe.

3. EXPERIMENTAL SETUP AND METHODS OF SYNTHESIS AND CHARACTERISATION

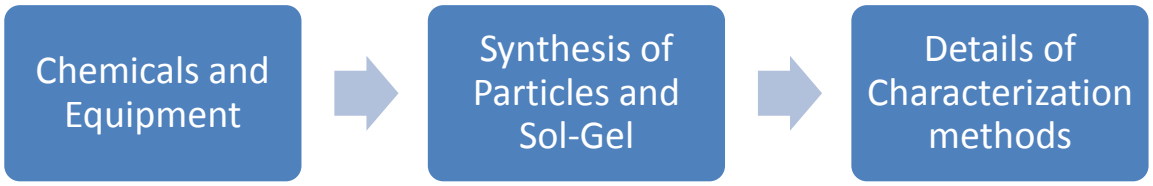

3.1. CHEMICALS

Table 3 shows a list of the chemicals used in the experiments with their respective names, abbreviations or formulas as the chemicals will be referred to later on. The purity of the samples as well as distributor used is also reported.

Table 3 Chemicals used in the experiments

Name	Abbreviation/ Formula	Purity (%)	Distributor
Bromethyl blue	BTB	N.A	Merck
Chloroform	$CHCl_3$	99	Merck
Cyclohexane	c.h	99	Lind
Dimethyloctadecyl[3-(trimethoxysilyl)propyl] ammonium chloride	ODAC-TMOS	72	VWR
Erbium (III) nitrate pentahydrate	$Er(NO_3)_3 \cdot 5H_2O$	99.9	Aldrich
Ethanol	EtOH	100	VWR

Methanol	MtOH		VWR
Neodymium (III) nitrate hexahydrate	$Nd(NO_3)_3 \cdot 5H_2O$	99.9	Aldrich
Oleic acid	OAc	100	Fluka
Oleyl amine	OAm	98	Aldrich
Silver oxide	Ag_2O	99	Aldrich
Sodium bicarbonate	$NaHCO_3$	-	KEBO Lab
Sodium fluoride	NaF	99	Sigma-Adrich
Sodium hydroxide	NaOH	98	Eka Nobel
Sodium yttrium fluoride, ytterbium and erbium doped	Commercial $NaYF_4$:Yb,Er	99	Sigma-Adrich
Tetrahydrofuran	THF	99.86	VWR
Tetraoctylammonium bromide	TOABr	98	Aldrich
Trimetoxy(octadecyl) silane	TMOS	90	Aldrich
Toluene	C_7H_8	100	VWR
Ytterbium (III) nitrate pentahydrate	$Yb(NO_3)_3 \cdot 5H_2O$	99.9	Aldrich
Yttrium (III) nitrate pentahydrate	$Y(NO_3)_3 \cdot 5H_2O$	99.8	Aldrich

3.2. EQUIPMENT

Glass wear such as measuring cylinders and beakers were used for the synthesis. In the oven the solution was in 40 ml Teflon liners in steel autoclaves as seen in Figure 16.

Figure 16 Picture of autoclave (left) and Teflon liner (right) used for the synthesis of the particles. The Teflon liner has an inner volume of 40 ml

For the post-treatment of the particles Labinco stirrer, Rotina 35 sentrifuge and Branson 3510 sonicator were used, as shown in Figure 17.

Figure 17 Picture of the three machines used for washing and isolation of the particles. From the left Labinco L 46 stirrer, Rotina 35 sentrigue and Branson 3510 sonicator

3.3. SYNTHESIS OF UPCONVERTING PARTICLES WITH CORE AND CORE-SHELL STRUCTURES

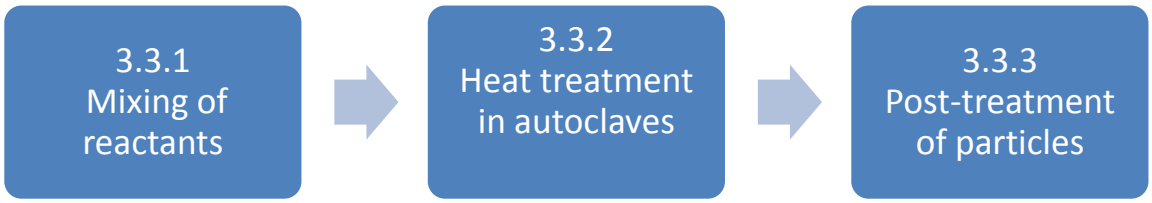

In this project there are three different synthesis methods that has been used to produce $NaYF_4$:Yb,Er, but the washing and isolation of the samples are all the same as explained in 3.3.3. The methods are based on the procedures reported by Sun et al. and Zhang et al. [8, 14]. The reported amounts are given for synthesising material in four autoclaves. The variations of the synthesis parameters can be found in Table 4 -

Table 6 in chapter 3.3.2

3.3.1. SOLVOTHERMAL METHOD FOR SYNTHESIS OF CORE PARTICLES

The lanthanide nitrate precursors and sodium fluoride solution were made by dissolving the powder in type II water in volumetric flasks of appropriate sizes.

3.3.1.A. PROCEDURE OF METHOD A

3.82 g NaOH was dissolved by magnetic stirring in 16 ml type II water and 22.4 ml EtOH. 64 ml oleic acid (OAc) was added under continuous stirring. The lanthanide

nitrate precursors, 3.04 ml 0.5M $Y(NO_3)_3$ (aq), 240 µl 0.2M $Yb(NO_3)_3$(aq), 160 µl 0.2M $Er(NO_3)_3$ (aq), were added and 25.6 ml 1M NaF (aq) was added dropwise to the solution.

The solution was left to stir for 20-30 minutes, poured into the autoclaves and placed in a preheated oven. After the heat treatment as reported in Table 4, the autoclaves were left to cool overnight. Then the post-treatment of the particles was done as explained in 3.3.3.

3.3.1.B. PROCEDURE OF METHOD B

2.85 g NaOH was dissolved by magnetic stirring for several hours in 40 g EtOH. 28.4 ml OAc and 33.2 ml 0.58M NaF (aq) was added. The solution was stirred until the solution turned transparent. Then the lanthanide nitrate precursors, 4.40 ml 0.80M $Y(NO_3)_3$(aq), 1.40 ml 0.63M $Yb(NO_3)_3$(aq), 0.20ml 0.40 M $Er(NO_3)_3$ (aq), were added. The solution was left to stir for 20-30 minutes, poured into the autoclaves and placed in a preheated oven. After the heat treatment as reported in Table 5, the autoclaves were left to cool overnight. Then the post-treatment of the particles was done as explained in 3.3.3.

3.3.1.C. PROCEDURE OF METHOD C

3.82 g NaOH was dissolved in 22.4 ml EtOH by magnetic stirrer. 64 ml OAc and 25.6 ml 1M NaF (aq) was added during continuous stirring. Then the lanthanide nitrate precursors, 3.04 ml 0.5M $Y(NO_3)_3$(aq), 240 µl 0.2M $Yb(NO_3)_3$(aq), 160 µl 0.2M $Er(NO_3)_3$(aq), were added. The solution was left to stir for 20-30 minutes, poured into the autoclaves and placed in a preheated oven. After the heat treatment as reported in

Table 6, the autoclaves were left to cool overnight. Then the post-treatment of the particles was done as explained in 3.3.3.

3.3.1.D. PROCEDURE FOR METHOD D

3.82 g NaOH was dissolved in 22.4 ml EtOH by magnetic stirrer. 64 ml OAc and 25.6 ml 1M NaF (aq) was added during continuous stirring. Then the lanthanide nitrate precursors,

6.08 ml 0.5M $Y(NO_3)_3$(aq), 480 µl 0.2M $Yb(NO_3)_3$(aq), 320 µl 0.2M $Er(NO_3)_3$(aq), were added. The solution was left to stir for 20-30 minutes, poured into the autoclaves and placed in a preheated oven. After the heat treatment as reported in

Table 6, the autoclaves were left to cool overnight. Then the post-treatment of the particles was done as explained in 3.3.3.

3.3.2. PARAMETERS OF THE SYNTHESES IN THE AUTOCLAVES

Tables 4-6 show the synthesis parameters used for the various samples synthesized.

Table 4 Variations in temperature, time and amount of surfactant for the synthesis method A

Name of sample	Temperature in oven /^{0}C	Time in oven /h	Amount of OAc /ml	Amount of OAm /ml
A1	210	24	64	-
A2	210	20	64	-
A3	210	20	32	-
A4	190	20	64	-
A5	170	20	64	-
A6	200	24	48	16
A7	200	24	42	21

Table 5 Variations in temperature, time and amount of surfactant for the synthesis method B

Name of sample	Temperature in oven /^{0}C	Time in oven /h	Amount of OAc /ml
B_core	210	24	28.4
B_core-shell	210	24	28.4

Table 6 Variations in temperature, time and amount of surfactant for the synthesis method C and D

Name of sample	Temperature in the oven /^{0}C	Time in the oven /h	Amount of OAc /ml	Amount of OAm /ml
C1	210	24	64	-
C2	210	24	64	-
C3	190	24	64	-
C4	190	24	64	-
C5	200	24	64	-
C6	210	24	32	32
D1	210	24	64	-

3.3.3. WASHING AND ISOLATING THE PARTICLES

The top liquid layer was poured out and the product at the bottom of the liner collected. To the product from two autoclaves, was dispersed in 10 ml cyclohexane (c.h) by sonication for 30 minutes. 20 ml EtOH was added before centrifugation (8000rpm x 6min). The product gathered as a white pellet in the bottom of the centrifuge tube. The liquid was poured off and 10 ml c.h added. The pellet was dispersed by stirring by Labinco L 46. Then sonication and centrifugations was repeated as described above. This was done three times. Finally the product was dispersed in c.h for further characterization or treatment.

3.4. HEAT-UP METHOD FOR SYNTHESIS OF CORE-SHELL PARTICLES

The heat-up method simply refers to precursors of the core sample being introduced to a new synthesis, thereby heating up the sample once again and obtaining a shell on the core particles [18]. The amount corresponding to the product of two autoclaves of the core-particles were dissolved in 5 ml OAc after the after-treatment and sonicated for 1h. The samples are treated the same way as the core samples, 3.3.3.

3.4.1.A. CORE-SHELL METHOD B

2.85 g NaOH was dissolved by magnetic stirring for several hours in 40 g EtOH. 23.4 ml OAc, 5 ml of the core-OAc mixture and 33.2 ml 0.58M NaF (aq) was added. The solution was stirred until the solution turned transparent. Then the lanthanide nitrate precursors, 4.40 ml 0.80M $Y(NO_3)_3$(aq) and 1.40 ml 0.63M $Nd(NO_3)_3$(aq), were added. The solution was left to stir for 20-30 minutes, poured into the autoclaves and placed in a preheated oven. The standard was set to 210^0C in the oven with time of 24h. The autoclaves were left to cool overnight.

3.4.1.B. CORE-SHELLS OF METHOD C

3.82 g NaOH was dissolved in 22.4 ml EtOH by magnetic stirrer. 59 ml OAc, 5 ml of the core-OAc mixture and 25.6 ml 1M NaF (aq) was added during continuous stirring. Then the lanthanide nitrate precursors, 3.04 ml 0.5M $Y(NO_3)_3$(aq), 240 µl 0.2M $Nd(NO_3)_3$(aq), were added. The solution was left to stir for 20-30 minutes, poured into the autoclaves and placed in a preheated oven. The standard was set to 210^0C in the oven with time of 24h. The autoclaves were left to cool overnight.

3.5. THE SENSING FILM

There are several components that make up the sensing film as shown in the illustration below. The synthesis of these will each be presented before the mixing of the final product, and are based on the work by Kringberg [26].

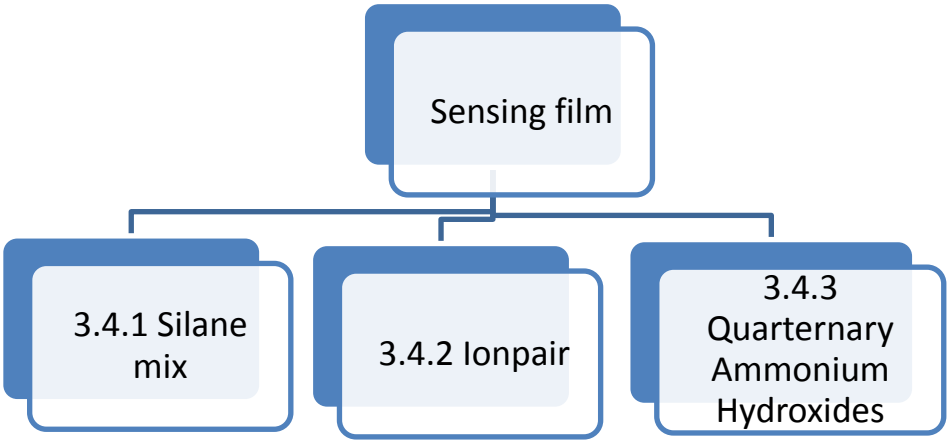

3.5.1. MIXING OF THE SILANES

The sol was made by mixing the following reactants of Table 7 in a plastic vial, and stirred for 3h by magnetic stirring.

Table 7 The reagents used to make the sol together with the respective amounts

Reagents	Volume /µl
TEOS	240
C3-TMOS	120
TFP-TMOS	120
OD-TMOS	120
THF	200
Toluene	800
HCl (aq) 0,1 M	160

3.5.2. SYNTHESIS OF IONPAIR

Cresol purple (CP) was dissolved in water by stirring for several hours. ODAC-TMOS and NaOH was added and the solution left to stir over night. The solution was diluted and filtered by use of filter paper and a Büchner funnel. After drying the ion-pair, CP-ODA, is dissolved in EtOH giving a 1.29mM solution.

BTB was dissolved in 0.1 M NaOH (aq). TOABr was disolved in 5ml toluene. The two solutions were stirred separately for 30 minutes and then together for an hour. The two phases were left to separate. 10 ml 0.1 M NaOH (aq) was used to wash the organic phase (blue) three times. The two phases were again left to separate and the blue layer extracted.

Table 8 Reagents used to make the ionpairs of CP-ODA and BTB-TOA with the respective amounts

Reagent	CP-ODA	BTB-TOA
Cresol Purple	0.039g	-
Water	50mL	-
72% ODAC-TMOS	0.511g	-
1M NaOH (aq)	300µL	-
Bromethyl Blue	-	0.062 g
0.1 M NaOH (aq)	-	10 ml
TOABr	-	0.11 g
Toluene	-	5 ml

3.5.3. SYNTHESIS OF QUATERNARY AMMONIUM HYDROXIDES

Dimethyloctadecyl[3-(trimethoxysilyl)propyl]ammonium hydroxide (ODAOH-TMOS) and tetraoctylammonium hydroxide (TOAOH) were synthesised by reacting 72% dimethyloctadecyl[3-(trimethoxysilyl)propyl]ammonium chloride (ODAC-TMOS) or tetraoctylammonium bromide (TOABr) respectively with silveroxide in methanol. The two solutions were each filtered through 0.45 µm Milliex® (PVDF, 33mm), and stored in a cool and dark place.

Table 9 The reagents used to make the hydroxides together with the respective amounts

Reactants	TOAOH	ODAOH-TMOS
Ag_2O	0.393 g	0.256 g
MeOH	4 ml	4 ml
TOABr	0.571 g	-
ODAC-TMOS (72%)	-	0.710 g

3.5.4. PREPARATION OF FILM

The silane mixture was mixed with chloroform, the ionpair and the UC particles dissolved in chloroform, see Table 10. The mixture was placed in sonication for 96 h and then by using a dropper put on a glass platelet for drying and further investigations.

Table 10 The reagents used to make the film together with the respective amounts

Reagents	Volume /µl
Sol	50
Chloroform	120
ODAOH-TMOS	60
TOAOH	40
Ion pair	250
UC particles*	250 of 0.02g UCP dissolved in 1ml chloroform.

***the film containing CP-ODA does not include UCPs**

3.6.CHARACTERIZATION OF PARTICLES

3.6.1. SCANNING ELECTRON MICROSCOPY

To investigate the products from method A at temperatures 170^0C and 190^0C, the instrument Quanta 200F (Fei) was used. Electron voltage of 20 kV and low vacuum mode was used and the stage set to 10 mm. Sample preparation: The samples were dried, crushed and dispersed on a carbon tape.

The instrument used for the rest of the samples was HITACHI SU8230. The stage was set to 8.8, 4.5, 2.6 or 2.2 mm. Electron voltage of 10 kV and low vacuum mode was used. For some samples deceleration mode was applied to enhance surface resolution and the electron voltage of 1 kV was used. Sample preparation: The solution was diluted and a drop was placed on a carbon covered copper grid and left to dry.

3.6.2. X-RAY DIFFRACTION

The instrument used was Bruker D8 Discover. The geometry is Bragg-Brentano and the x-ray radiation is $\lambda = 0.15406$ nm. The 2θ values were taken from 10^0 to 70^0. The results were compared with the crystallographic database in the software EVA and extracted by PowDLL converter to the software Origin for data processing. Sample preparation: The samples were dropped on the XRD holder and left to evaporate the solvent.

3.6.3. TRANSMISSION ELECTRON MICROSCOPY

The instrument, JEM-2100F, was operated by Phoung Dan Nguyen. Both selected area diffraction and scanning transmission mode was adopted. The electron voltage was 200 kV. For spot analysis by EDS, the spot size of the beam was changed from 1 nm to 0.5. Sample preparation: The solution was diluted and a drop was placed on a holey carbon covered copper grid.

3.6.4. X-RAY PHOTON SPECTROSCOPY

The instrument, KRATOS AXIS ULTRA^{DLD}, was operated by Spyros Diplas. Monochromatic Al Kα radiation was used as excitation source, vacuum of 10^{-9} mbar and a charge neutraliser was applied. The results were analysed in the software CasaXPS. Sample preparation: The samples were dried, crushed and put on a cobber sample holder.

3.7. MEASUREMENTS OF OPTICAL PROPERTIES

The core particles were excited by 980 nm laser and the core-shell particles by 808 nm laser from Roithner Lasertechnik. The measurements were performed in a dark room. In the given setup with optical fibres the excitation power is estimated to give 2.3 Wcm^{-1}. The driver of the lasers was a made in-house and the circuit is shown in Appendix D – The Laserdrive. Separate laser and detector probes were used to study the particles in solution, whereas for the dry samples a combined probe was applied as shown in figure 21 A) and B) respectively. For the setup in B) the laser was connected to an optical fiber which is split and also connected to the spectrometer. Both the incoming light and the detected light from the sample therefore enter and exit the same probe. The setup is shown in Figure 18. The results were mapped in the software Avasoft 7.3.1 and extracted to the software Origin for data processing. Sample preparation: Particles in solution were used directly as prepared by the synthesis. Dry samples were deposited by dropper on a microscope glass slide and left to dry.

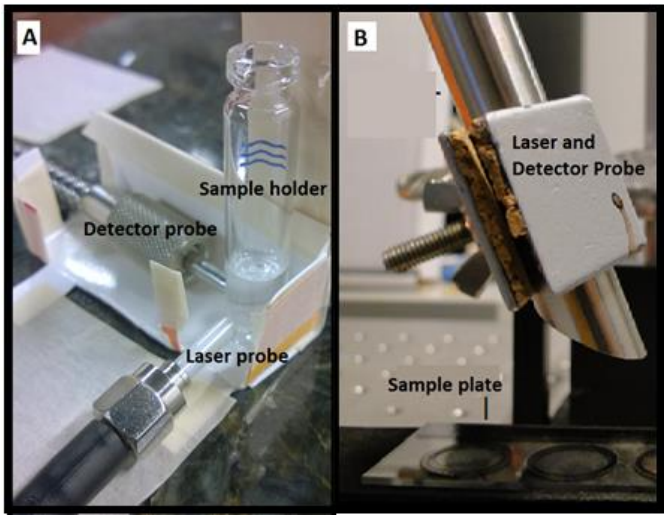

Figure 18 The experimental setup for wet and dry samples in images A) and B) respectively

4. RESULTS AND DISCUSSION

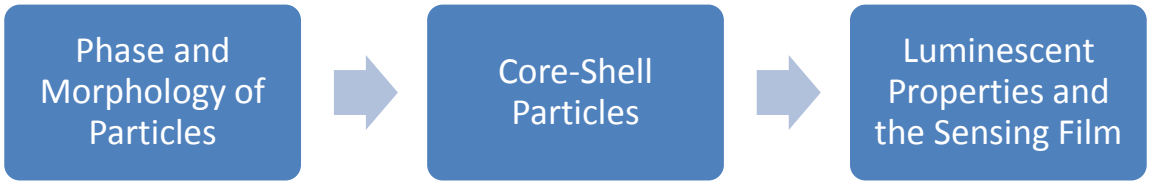

In section 4.1 The SEM and XRD results with respect to variations of each method A-D are presented and discussed. The core-shell particles of method C are discussed separately in section 4.2 as these were also studied by XPS and TEM. Then an overview of the optical properties of the various samples is given (4.3), followed by the results of the sensing element (4.4).

4.1. MORPHOLOGY, SIZE AND PHASES OF THE PARTICLES

A first impression of the success of the various synthesis methods is given by the SEM images (micrographs). These give information on the size and morphology of the particles. This is illustrated in Figure 19 where micrographs of the standard samples of methods A-D are shown. Then by studying the micrographs in relation to the XRD-results of the samples, the effect of the different synthesis parameters may be discussed.

As mentioned in the introduction, the hexagonal phase of $NaYF_4$ doped with Yb^{3+} and Er^{3+} (β-$NaYF_4$:Yb,Er) is the most effective UC material for green upconversion and is therefore also the desired product of the syntheses performed in the thesis. The actual obtained phase of the particles will be given by analysis of X-ray diffractograms; however the morphology observed from SEM images of the crystal can also give an indication of the phase. That is because the atomic arrangement in the structure is reflected in the shape of the crystal [41], given the hexagonal phase a macroscopic hexagonal shape is predicted. Rods have a lower surface area-to-volume ratio than spherical particles resulting in higher UC effectivity [8]. Seeing as the products of both

articles on which the synthesis methods are based on are rods, the expected results are hexagonal rods [8, 27].

The standard reaction time and temperature of all the methods was set to 210 ^{0}C and 24h. That was chosen based on the article by Zhang which clearly illustrates the effects of temperature and time on the transition from α- to β-$NaYF_4$ [14]. In particular the article shows the development of XRD patterns for a 12h synthesis varying the temperature (130-260 ^{0}C) and another figure of a synthesis at 180 ^{0}C with varying time (3-96h). Pure hexagonal phase was obtained at 230 ^{0}C for 12h and after 48h for 180 ^{0}C. Thereby using the parameters 210^{0}C and 24h should be sufficient to synthesise pure β-$NaYF_4$.

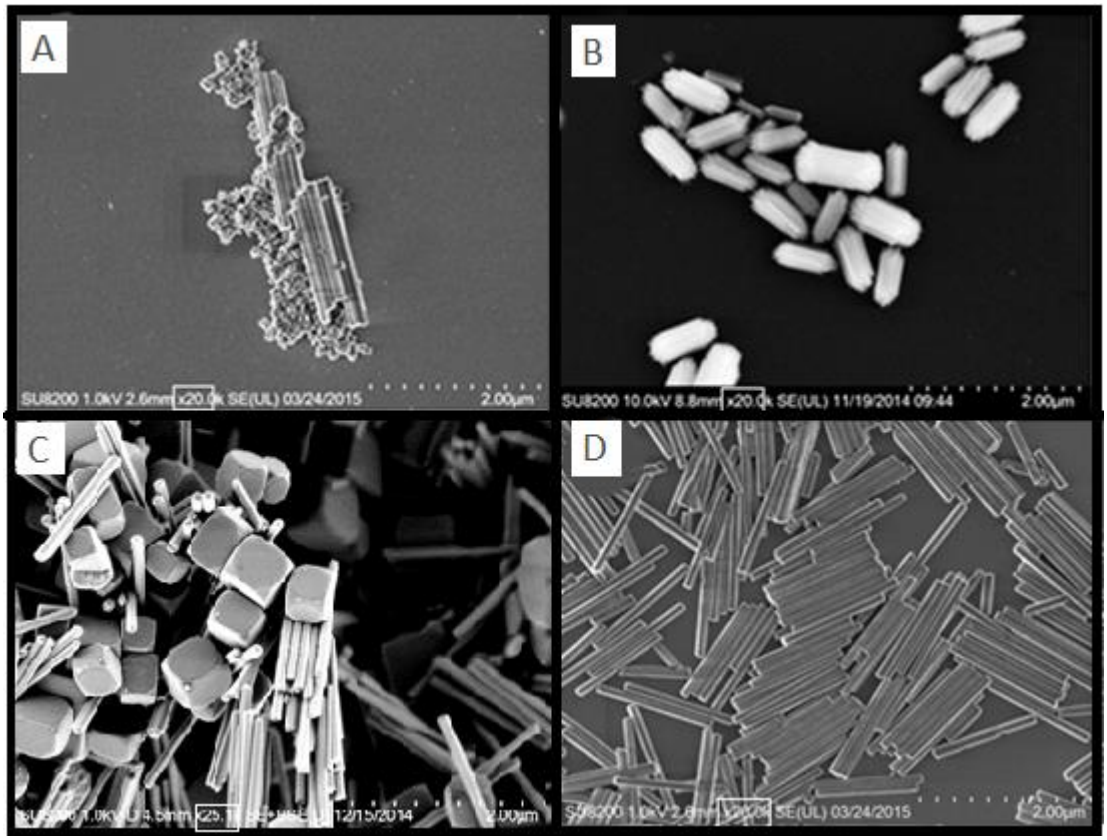

Figure 19 SEM images of the standard (210^{0}C, 24h) of each synthesis method A-D, with similar magnifications. Figure A)-D) corresponds to method A – D respectively. Methods C and D are new methods developed as a part of this project.

4.1.1. METHOD A

Method A is a reproduction of Sun et al.'s procedure [8] and produces the expected hexagonal rods. Figure 20 is the SEM results obtained of the standard sample of method A. It shows that there is a significant size distribution of the rods (about 1.2-3.0 µm) and a large amount of another compound. By further SEM investigations of the standard sample of method A, Figure 22 C) and D), it can be seen that the substance surrounding the rods is made up of nanoscopic cubes. D) also reveals some more of the morphology of the rods. There are clear edges along the length of the rod, indicating a hexagonal shape of the crystal corresponding to the hexagonal crystal structure of β-$NaYF_4$.

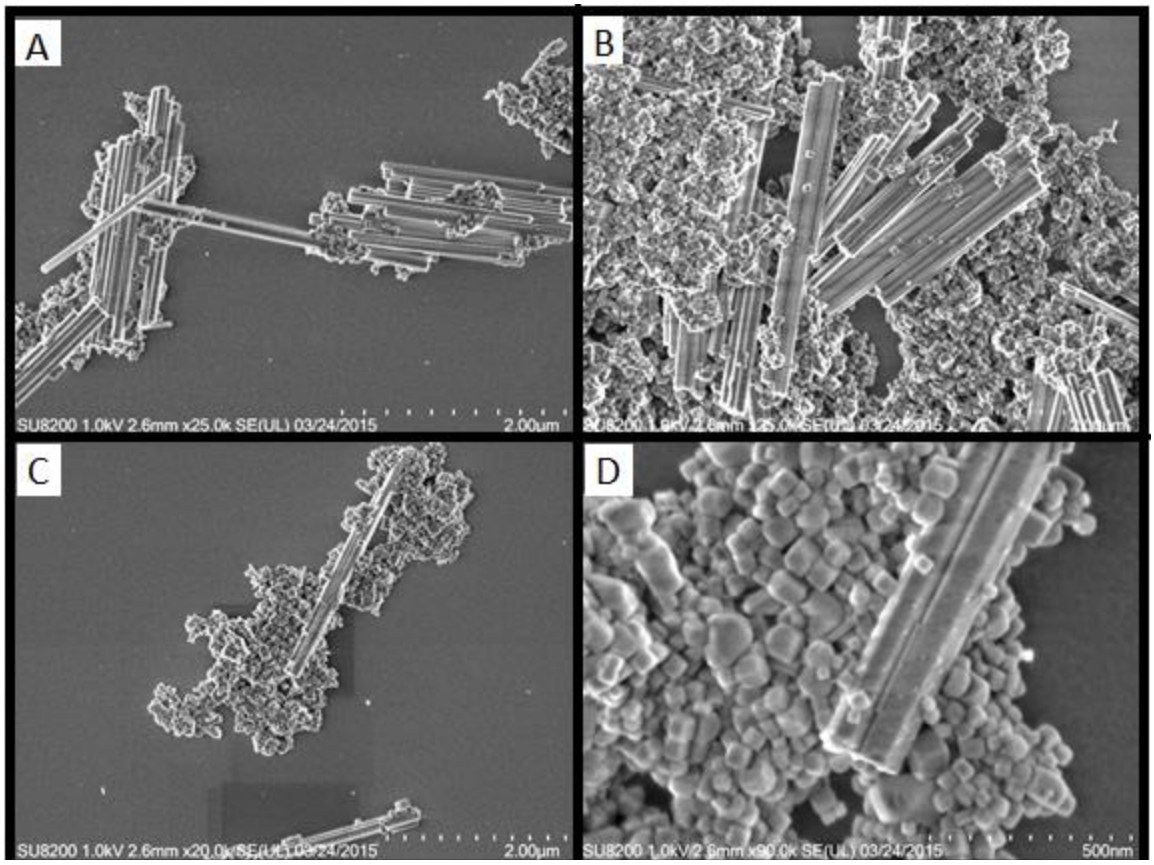

Figure 20 SEM images of standard sample of method A. A) and B) together shows the morphology and sizes of the sample in general, with rods of varying sizes surrounded by another compound. D) is an enlargement of the tip of the rod in C) and shows hexagonal rods surrounded by nanoscopic cubes.

In Sun's article they report uniform rods of 950 nm in length and the presence of nanoparticles after a treatment of 24h at 190^0C. The article does not refer to what compound these nanoparticles are, simply that they seem to disappear after several rounds of washing. [8]

The XRD-measurements for the standard sample in Figure 23, reveals that there is sodium fluoride (NaF) present. However, the sample produced by the same batch but only left in the oven for 20h also have a peak characteristic of α-$NaYF_4$, marked by a square in Figure 21. Although the characteristic feature of diffractograms for samples containing both α- and β-$NaYF_4$ is four successive peaks around $2\theta = 30$, the peak around $2\theta = 28$ is sufficient to conclude that there is α-$NaYF_4$ present, as the other peak around $2\theta = 32$ could be weaker and there is in general a poor count rate for the measurements. The result fits with the one reported by Liu et al. [34]. Their XRD results for the NaF-to-Ln^{3+} ratio of 12 shows all of the same phases, namely β-$NaYF_4$, α-$NaYF_4$ and NaF. The NaF-to-Ln^{3+} ratio of method A is 16.

Both Zhang et al. and Ding et al. who investigated the phase transitions of $NaYF_4$ with regards to temperature and time found that first there first is only α-$NaYF_4$ present, then a mix of the two phases and eventually pure β-$NaYF_4$ [27, 28]. Given the α-$NaYF_4$ peak present at the sample prepare for 20h and not for 24h of the batch synthesized at 210^0C it seems that our estimation derived from the study by Zhang et al. was right, that the combination of 210^0C and 24h gives pure β-$NaYF_4$ for the system.

Another feature of the micrographs of Figure 20 is the alignment of rods in aggregates. This might indicate that the surfactant functions only to direct the growth of the crystals, but does not contribute to keeping the particles separate. This also explains the difficulty observed in dispersing the particles to form a colloidal solution. Some articles refer to this as self-assembly of $NaYF_4$ [14, 42]. Ding et al. also observed large arrangements of agglomerated rods and called these large-scale ordered 2D nanoarrays [28].

Both SEM and XRD results of sample of method A synthesised with only half the amount of surfactant are presented in Figure 21. The micrograph shows rods that are much smaller than the ones in Figure 20. Despite the low intensity, the diffractogram shown in Figure 21 C) shows the characteristic peaks of β-$NaYF_4$. The big sircle in the middle of Figure 21A), is believed to be an area made up of NaF, and the assumption is supported by the NaF peaks marked by 'X' in the diffractogram to the right.

The surfactant oleic acid (OAc) also has a function as the solvent of the reaction in method A. However, it was believed to be in large excess and therefore the synthesis with half the amount of OAc was performed. As seen in Figure 21A) and B) this resulted in rods which are less than 500 nm in length and that seem not to have aglomerated as with the standard sample of method A. This is a promising result, however there is still quite a large size distribution of the particles.

Inspired by Zhang et al. [14], temperature variations of 170-210^{0}C in the oven were investigated for method A. Figure 22 shows the SEM images and diffractograms of the respective samples. Although the micrographs B) and C) in Figure 22 are of worse quality than micrograph A), it is possible to remark that they are quite similar. There are

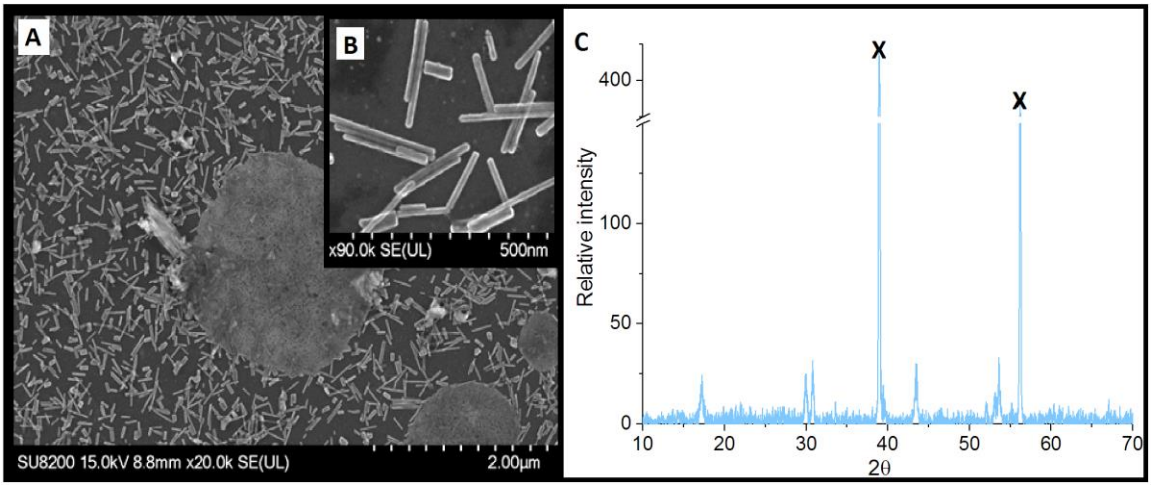

Figure 21 A) and B) are SEM images of the sample prepared by method A, but with half the amount of surfactant as compared to the standard sample. The inset B) is a further magnification of the same sample. C) is a diffractogram of the sample showing the presence of β-$NaYF_4$ and the peaks marked by X belong to the phase of cubic NaF.

several different morphologies present in all of the samples. The most noteworthy is the presence of large cubes, small rods and an even smaller compound which resembles the nanoscopic cubes of Figure 20. Some of the rods in the samples prepared at 170^0C and 190^0C resemble nanowires as these are very small and with large aspect ratios.

Both similarities and differences of the three samples are also shown in the diffractograms in Figure 22. The β-$NaYF_4$ peaks of the samples at 170^0C and 190^0C are wider than those of 210^0C, indicating smaller sizes or possibly a less ordered crystal structure of the particles prepared at lower temperatures. Also the relative intensities of the peaks are different, indicating differences in shape. All the samples show peaks corresponding to NaF as well. These are marked by an 'X' each. The 210^0C sample also has a higher count rate, however this does not explain the presence of an extra peak at 2θ~28 compared to the diffractograms of the lower temperatures. This peak is characteristic for α-$NaYF_4$ as explained previously. With reference to the results obtained by Zhang et al. it should be noted that it is strange that the samples prepared at lower temperatures do not also show the α-$NaYF_4$ peaks [14].

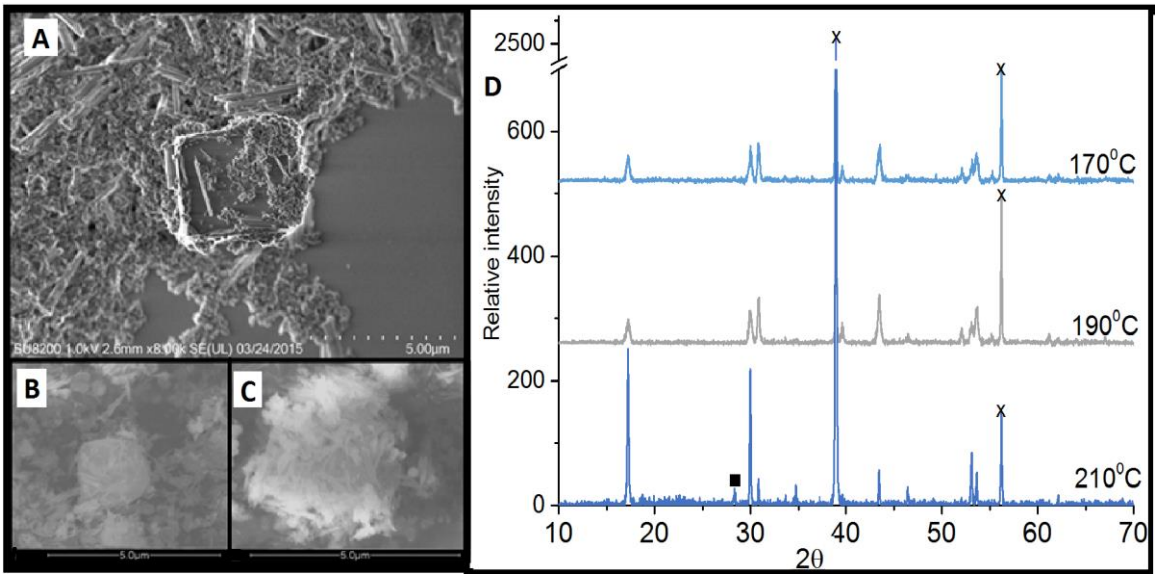

Figure 22 A)-C) are SEM images of the products of method A obtained after 20h at temperatures A) 210^0C, B) 190^0C and C) 170^0C. Image D) show the diffractograms of the three samples. There is a clear difference between the lower temperatures and 210^0C, especially in terms of relative intensities of the peaks. For all samples β-$NaYF_4$ is present and the peaks marked by X belong to the phase of cubic NaF

Oleyl amine (OAm) was applied together with OAc as solvent and surfactant in the synthesis of method A, Figure 23 show the XRD results of the syntheses. OAm is a surfactant that has been reported to facilitate the phase transition from α to β-$NaYF_4$ [13], and the pair of OAc and OAm has been used successfully in many syntheses of nanoparticles [43]. The ratios of OAc-to-OAm applied were three-to-one, and two-to-one. The diffractograms (Figure 23) show the presence of hexagonal $NaYF_4$:Yb,Er and cubic NaF, as for the previous samples. The more OAm present in the synthesis the broader and lower the diffraction peaks. A broadening of the peaks and lower relative intensities indicate smaller particles and lower crystalinitiy of the samples compared to the standard sample. There is also a change in the height differences of the various peaks, indicating different shapes of the particles Due to limited resources these were not investigated by SEM and because of the continued presence of NaF, method A was not investigated further.

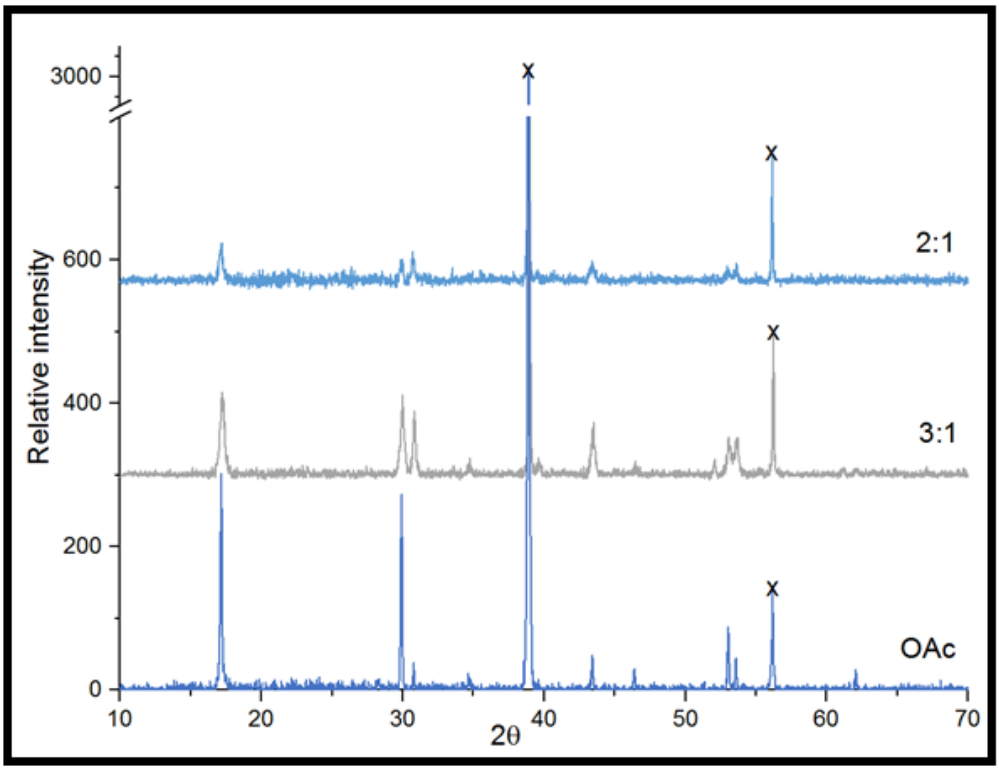

Figure 23 XRD results of the samples prepared by varying ratios of OAc to OAm. 2:1 and 3:1 refer to the OAc-to-OAm ratio used in the syntheses of the samples. The more OAm present, the broader the peaks and lower the count rate becomes, indicating smaller particles. For all samples β-$NaYF_4$ is present and the peaks marked by X belong to the phase of cubic NaF

4.1.2. METHOD B

Method B is taken from the previously mentioned article by Zhang et al. [14]. Figure 24 shows the SEM images of both core and core-shell particles synthesised by the method. The heat-up method for producing core-shell particles was applied for method B. The corresponding micrographs and XRD results are shown together with the core particles in figures 26 and 27. Images A) and B) are of the core sample. Image A) is taken in regular SEM mode, image B) in STEM mode. Images C) and D) are of the core-shell sample and deceleration was used to enhance the features of the surface of the particles. The experimental procedure seems to be fairly similar to method A. However, the concentration of the reactants as well as the order by which they were mixed is different, and by comparing the SEM results of Figure 24 to Figure 20 of method A it can be seen that the results are very different.

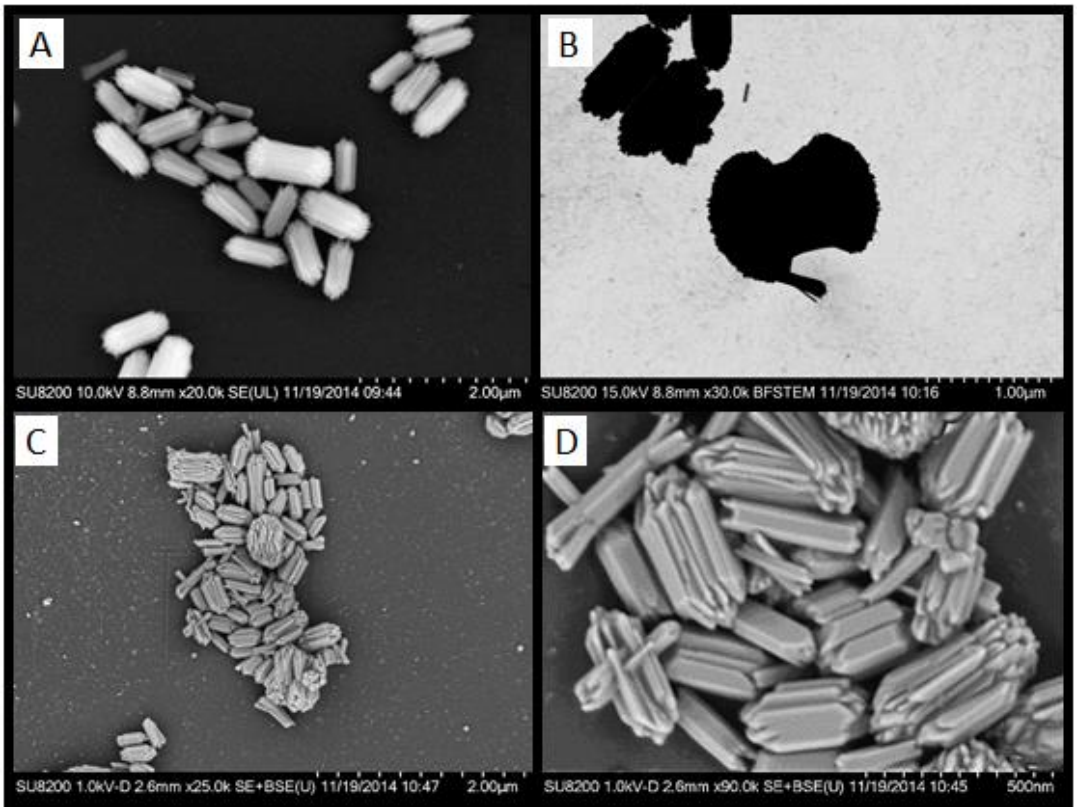

Figure 24 SEM images of the particles obtained by method B. Images A) and B) are SEM and STEM mode images respectively of the core particles. Image D) is a magnification of the same particles as in image C) both taken in SEM deceleration mode and pictures the core-shell particles of method B.

The morphology of the particles in Figure 24 resembles the hierarchical growth seen for fluoroapatite [9] or "nanobundles" of YF_3 [44]. Hierarchical growth evolves from thin, elongated shapes the structure to form aggregates in the shape of dumbbells, or bundles, and eventually spheres. Especially the STEM micrograph of image 26 B) resembles the intermediate stages of this process. The size of the particles are about 400 to 1000 nm, with most of the particles having a size of about 700-800 nm. For half the reaction time Zhang reports the synthesis of 500 nm nanotubes [14]. The size distribution of the particles seems to be more evenly distributed than what is the case of method A.

An interesting feature of method B is that the XRD-measurements in Figure 25 show no peaks for NaF, nor are there cubes present in the micrographs. The diffraction peaks are quite wide and the relative intensity of the (100) peak is huge, indicating that the particles are made up of rods. Repetitions of the experiment resulted in nearly identical diffractograms, see Appendix B – Extra results of Method B.

The core-shell particles are fairly similar to those of the core particles. It is noteworthy that the sizes of the core-shell particles are significantly shorter than the core particles, 200-700nm. This seems to make the assumption that there is a core-shell structure invalid, with regards to the shell forming a layer on the outside of the core particles, making them larger. That the size of the supposed core-shell particles is smaller than the standard sample can be explained by the presence of Nd. Chen et al. [45] observed that by using Nd^{3+} it was possible to produce smaller β-$NaYF_4$ particles at the same reaction parameters than without Nd^{3+} present.

A particle of each of the core and the core-shell samples were analyzed by EDS in the SEM. According to these measurements as summarized in

Table 11 there is no sodium (Na) present in the core-shell particles and only a small amount in the core particle. However, there is at least neodymium (Nd) present in the core-shell structure and not in the standard core-sample. The missing or low amounts of Na may be explained by dissolution of the ions from the crystals. Lisjak et. al has studied

the dissolution of several UC materials, and found that Na^+ was present in aqueous solution to a higher degree than the other ions [46].

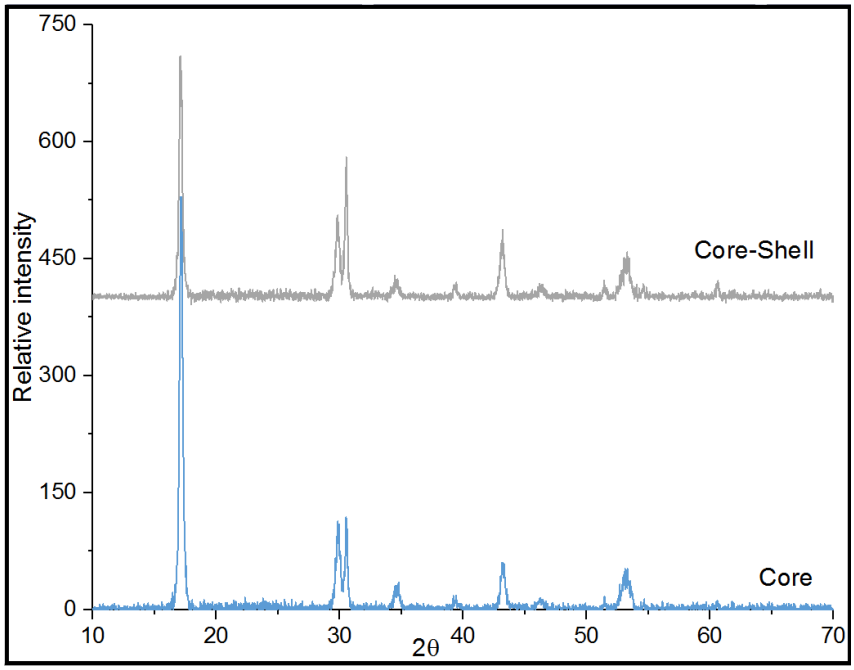

Figure 25 Diffractograms of both samples of method B corresponding to pure β-NaYF₄

Table 11 Atomic percentage of Na, Y, Nd, Yb, Er and F of B_standard and B_core-shell given from EDS measurements in SEM

Sample	Na	Y	F	Yb	Er	Nd
B_standard	3.68	35.19	47.72	11.12	2.29	-
B_core-shell	0	35.59	56.27	6.13	1.24	0.76

A final remark on the EDS results is the ratio of fluoride to the other elements which from the chemical formula should be 2 to 1, but is closer to 1. This is also off compared to the original article which reports stoichiometric relations [14].

4.1.3. METHOD C

Figure 26 shows the SEM images of the standard sample of method C, the results clearly show both rods and cubes. The diffractogram of the sample in Figure 27 shows the presence of both β-$NaYF_4$ and NaF. A striking difference between the micrographs of method A and C, Figure 20 and Figure 26 respectively, is the size of the NaF cubes. The cubes of method C are extremely large compared to those surrounding the rods of method A. Further comparison with method A gives that the size-distribution of the rods seem to be narrower, and the rods shorter. It is difficult to determine the exact size of the rods, given the spatial orientation of these in the SEM image, but they are estimated to be about 1µm long. There are also some rods at about half this size.

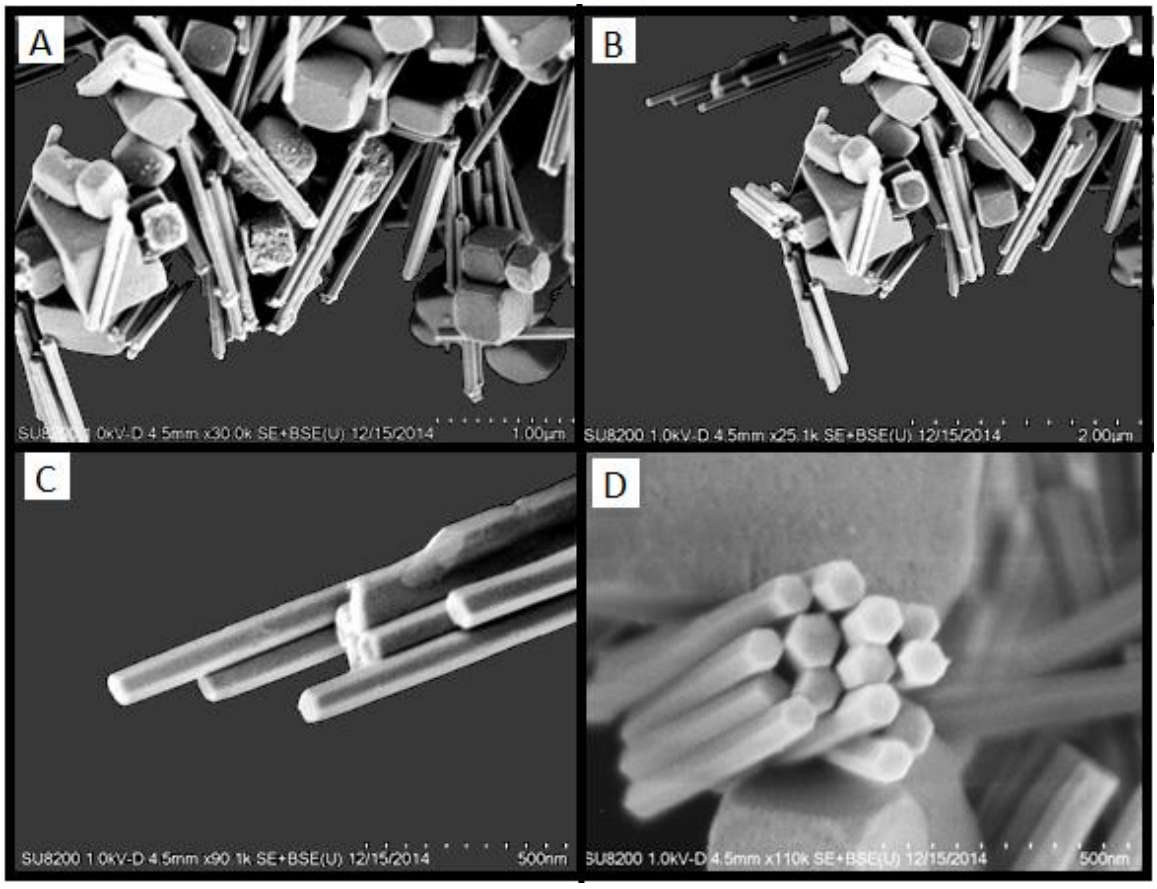

Figure 26 SEM images of various magnifications taken in deceleration mode of the standard sample of method C. There are rods and cubes, and from images C) and D) the rods are clearly hexagonal.

By increasing the magnification in the SEM, the morphology of the sample can be studied closer. A strong indication that the rods are made up of β-$NaYF_4$ is given by images C) and D) of Figure 26. These show that the rods of the sample are hexagonal in shape. The images in Figure 26 also show the agglomeration of aligned rods. As with method A, the cubes might be NaF or cubic $NaYF_4$. From the theory of dissolution-reconstruction of α-$NaYF_4$ to form β-$NaYF_4$ presented in the theory of the solvothermal method however, it is unlikely that α-$NaYF_4$ has grown to become large cubes. The diffractogram in Figure 27 confirms that there is β-$NaYF_4$ and NaF present in the sample, but no α-$NaYF_4$. An interesting feature of the cubes, visible in A), B) and D) in Figure 26, is the rounded corners caused by preferential growth of the crystal planes [9].

As with method A, a ratio of OAc and OAm as surfactants were investigated, a ratio of one-to-one was chosen. Figure 28 show the SEM results of the synthesis. The particles are very different from the other samples. There is a huge range of sizes from less than a micron to over 10μm and a variation of shapes including short rods and longer needles all with different aspect ratios. An interesting feature, seen in image B), is that the particles with the largest aspect ratios seem to have the morphology of tubes and not rods.

The XRD data in Figure 27 indicate that there is both α- and β-$NaYF_4$ present in the sample as well as NaF. The NaF peaks are marked by ‘X’. By using these peaks as reference, there seems to be a shift towards lower 2θ values of the peaks of $NaYF_4$. Given this shift and the change of relative intensities of the peaks compared to the standard sample, there is probably not α-$NaYF_4$ present in the sample after all. Because of the obvious poor control over size and morphology of the particles for the synthesis combining OAc and OAm the use of OAm was stopped. Instead the standard of method C was developed into the new method D.

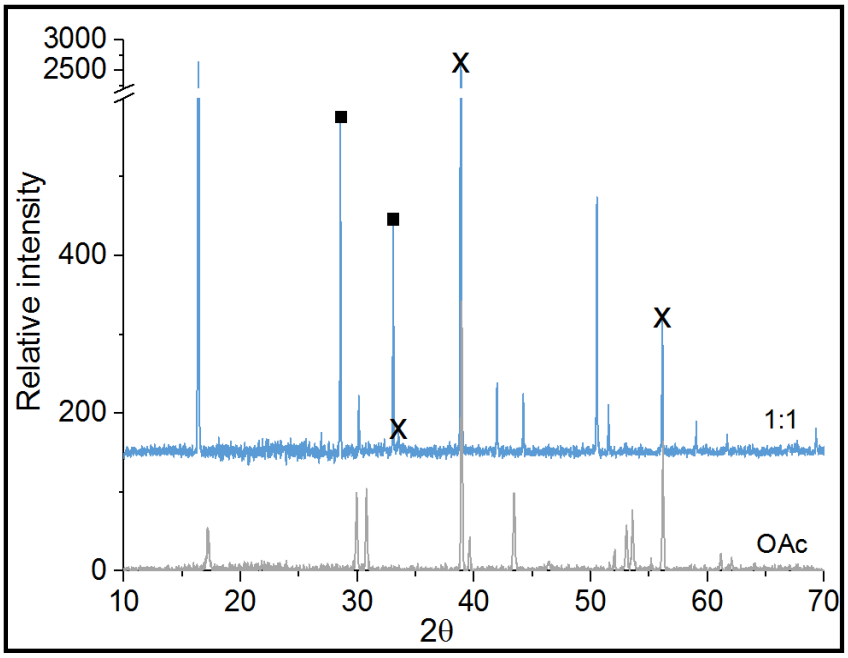

Figure 27 Diffractograms of the standard sample of method C marked by 'OAc' and the sample synthesized with a 1-to-1 ratio of OAc and OAm. The standard sample shows β-$NaYF_4$ and the peaks marked by X of cubic NaF and α- $NaYF_4$ peaks are marked by black squares in the figure.

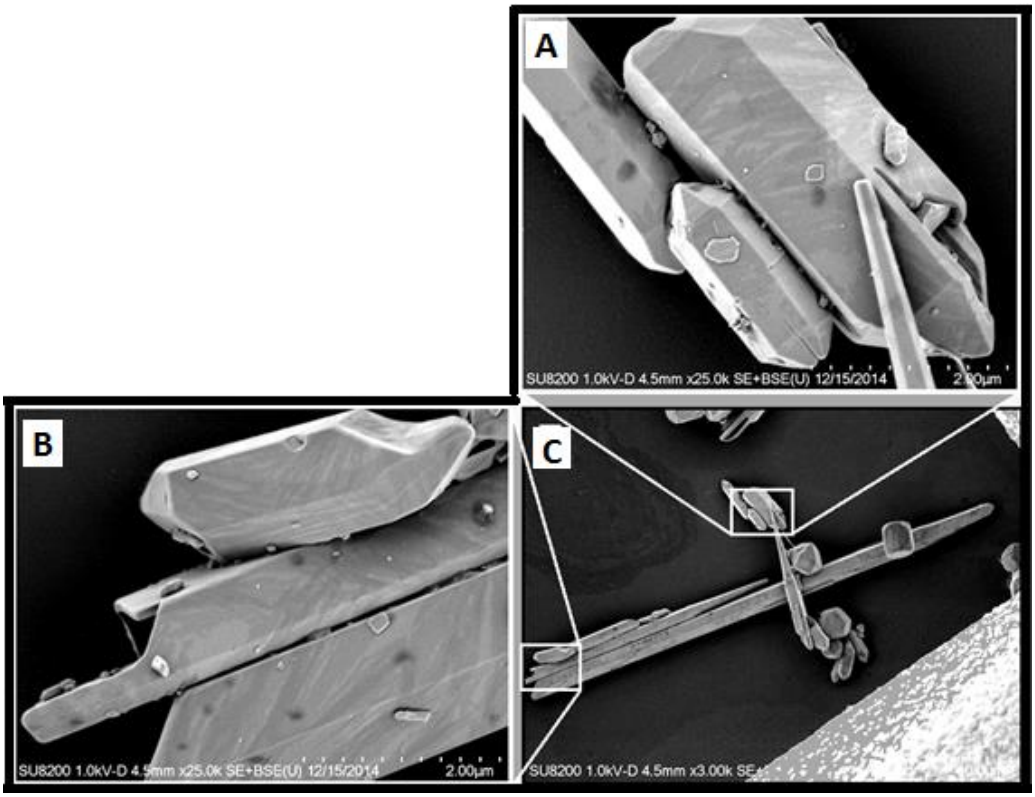

Figure 28 Micrographs of the sample of method C made with a 1-to-1 ratio of the surfactants OAc and OAm. B) and C) are higher magnifications of the areas indicated by the white squares. The figure illustrates the wide size distribution and various shapes of the particles in the sample.

4.1.4. METHOD D

The SEM results of method D are presented in Figure 29 which show a narrow size distribution of hexagonal rods with smooth surfaces of about 1.2-1.4 µm in length. The length was determined by measuring 175 of the rods in image 31 A). There are also some shorter rods as illustrated in image B)

Method D is an attempt to make method C more similar to method B and obtain β-$NaYF_4$ without NaF present. The ratio of lanthanide precursors to sodium fluoride solution was altered based on the thoughts that with a higher Ln^{3+} content, this would react with the excess NaF to produce $NaYF_4$. The new NaF-to-Ln^{3+} ratio is four as in method B instead of 16 which it was for methods A and C. Lieu et al reported that with a NaF-to-Ln^{3+} ratio

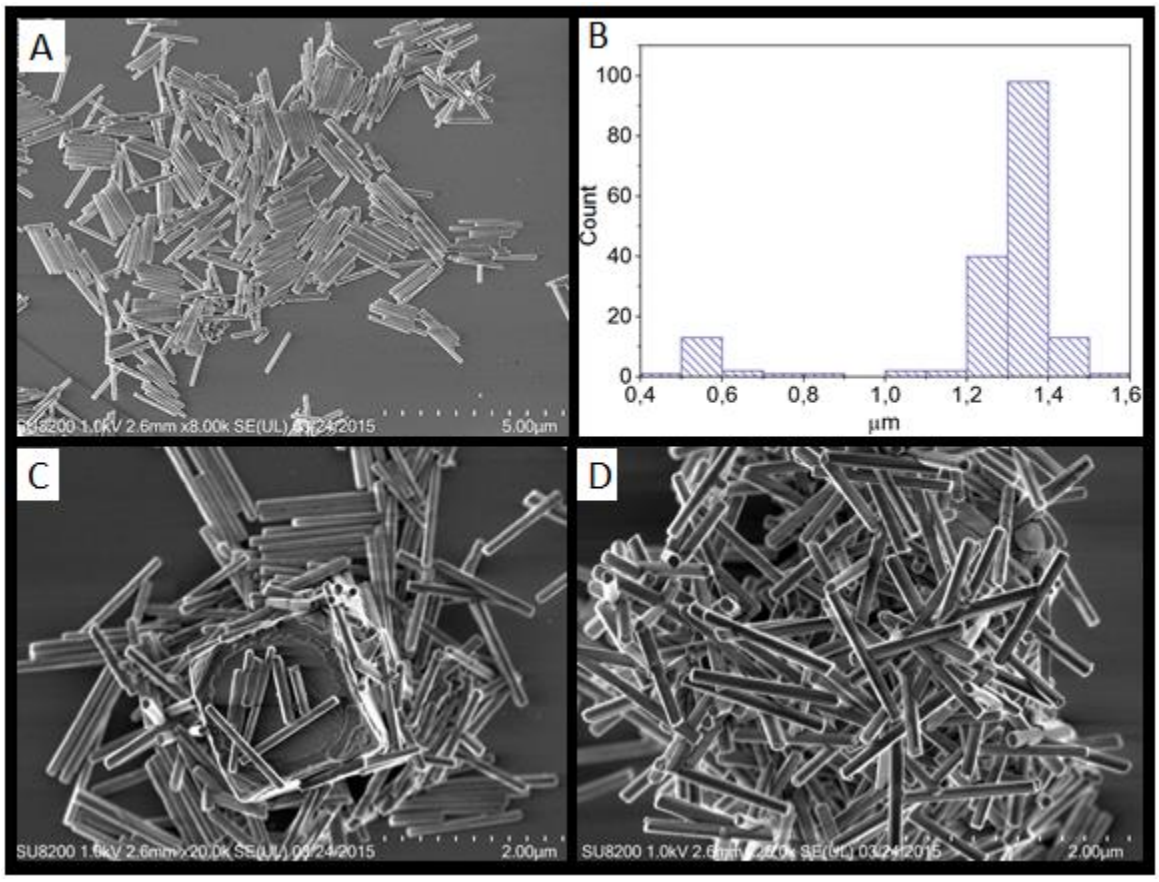

Figure 29 A), C) and D) are SEM images in deceleration mode of sample D. A) gives an overview whereas C) and D) are of equal magnification of different areas of the sample. B) shows the size distribution of the rods present in A).

of 6 the product was mainly α-$NaYF_4$ without the presence of NaF [34].

The XRD measurements, Figure 30, show that β-$NaYF_4$ has been synthesised and that there is still NaF present in the sample. Investigations by SEM show large cubes, such as image 31 C). however to a lesser extent than for method C. The diffractogram of method D is the only one of the methods which show all of the characteristic peaks of β-$NaYF_4$ and a good signal-to-noise ratio. The diffraction peaks are also narrow, indicating a high crystalinity of the sample.

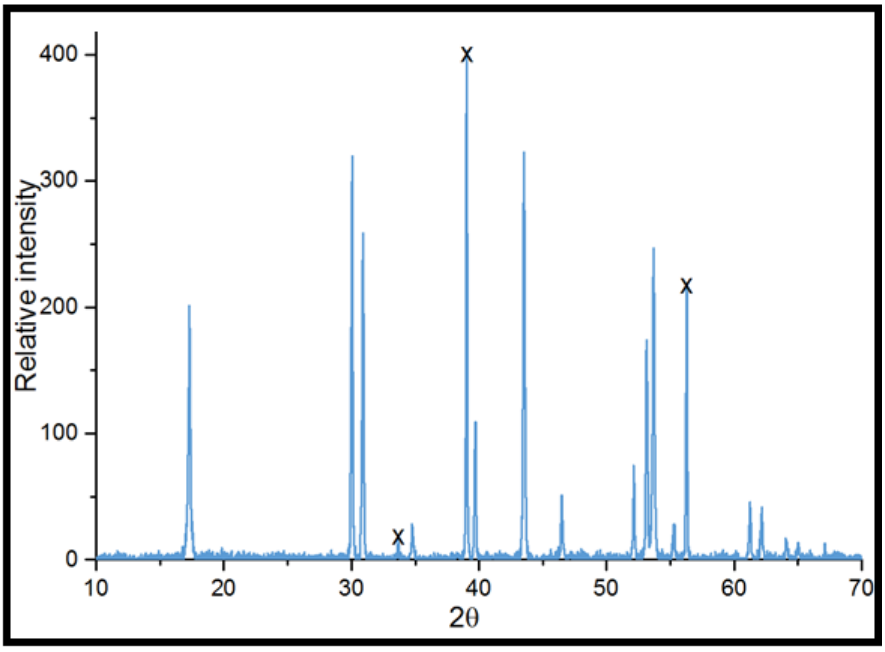

Figure 30 Diffractogram of method D, showing the characteristic peaks of β-$NaYF_4$ as well as peaks of NaF marked by X.

The SEM images of Figure 31 show close-ups of the rods of method D. It shows both an alignment of the rods as refered to earlier as an arrangements of agglomerated rods and called these large-scale ordered 2D nanoarrays [28] and another feature of small spheres at the end of the rods, such as for Figure 31A). This indicates that by a longer reaction time the rods could have grown longer but not wider.

After having investigated the tip of the rods, figure 33 A), the pattern of small particles on the rods in image B) could be seen. What has probably happened is that the focused electron beam of the SEM has heated the sample and that outside the focus of the beam the sample is still cool so that the material is deposited again. The pattern of deposited material coresponds in shape to the square left by the electron beam.

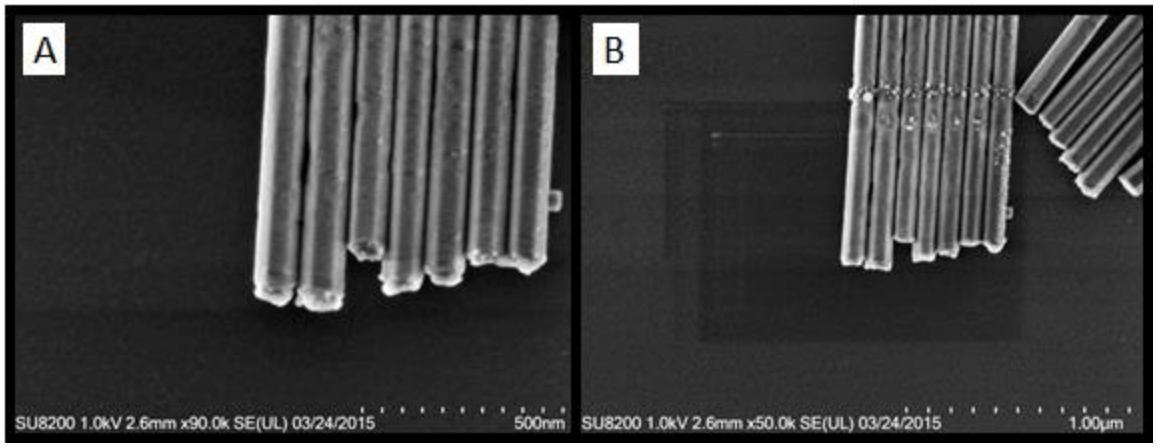

Figure 31 SEM images of high magnifications of standard sample of method D. There are small spheres at the end of the rods in A), indicating that the rods are still prone to growing longer. Image B) shows a deposition of material after heating by the electron beam

4.2. SUMMARY OF METHODS A-D

The results of size, phase and morphology variations of the synthesis methods together respective results of are shown in

Table 12 and schematic illustrations of the observed morphologies by SEM are depicted

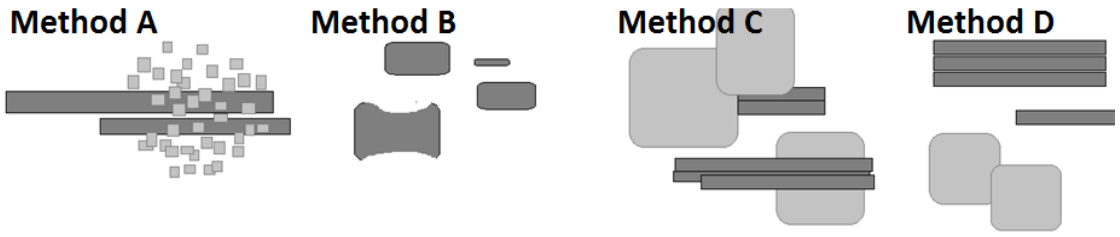

Figure 32 Schematic overview of the morphological results of the standard sample of methods A-D. The sizes are not to scale.

in Figure 32.

Table 12 Overview of the results of the various syntheses methods A-D. The product is determined by the phases present in XRD results and approximate sizes are estimated from SEM images.

Synthesis method	Temperature / ^{0}C	Surfactants	Product	Approximate Size range	Morphology
A	210	OAc	β-$NaYF_4$ + NaF	1.2-3µm	Rods, small cubes
	210	½ OAc	β-$NaYF_4$ + NaF	< 0.5 µm	Rods, small cubes
	190	OAc	β-$NaYF_4$ + NaF	-	Rods, needles, cubes
	170	OAc	β-$NaYF_4$ + NaF	-	Rods, needles, cubes
	200	3OAc : 1OAm	β-$NaYF_4$ + NaF	-	-
	200	2OAc : 1OAm	β-$NaYF_4$ + NaF	-	-
B	210	OAc	β-$NaYF_4$	0.4-1µm	Hierarchical assemblies
C	210	OAc	β-$NaYF_4$ + NaF	0.7-1.4µm	Rods, large cubes
	200	1OAc : 1OAm	β-$NaYF_4$ + NaF	2-14 µm	Rods of various aspect ratios
D	210	OAc	β-$NaYF_4$ + NaF	0.5-1.3µm	Rods, large cubes

4.3. THE CORE-SHELL STRUCTURE OF METHOD C

With the aim of making core-shell particles of $NaYF_4$:Yb,Er@$NaYF_4$:Nd, a new batch of method C at 190^0C and another at 210^0C was synthesized. The SEM results of both the core and the core-shell particles are shown in Figure 33 and Figure 34 for the samples synthesised at 190^0C and 210^0C respectively.

In Figure 33 images A) and B) are of the core samples. With the presence of welldefined, seemingly uniform in shape and size, rods and large cubes of various sizes, these show strong resemblance to the standard sample of method C in Figure 26. Images C) and D) show the core-shell sample and are different from the core particles, in particular because there are rods of several different sizes and aspect ratios. It seems plausible that the

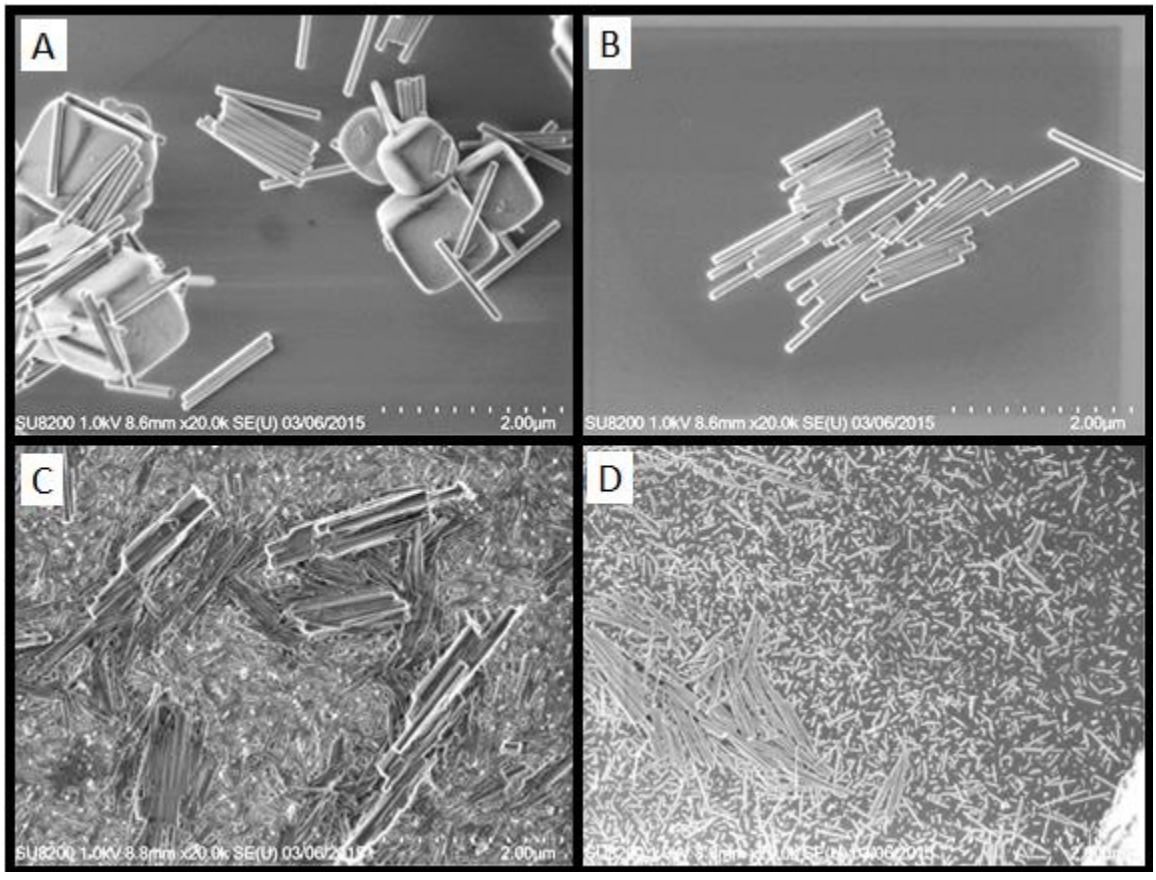

Figure 33 SEM images of the core [A) and B)] and core-shell [C) and D)] structure of method C synthesized at 190^0C. The SEM images are all of similar magnification. A) and B) shows similarities to the standard sample of method C. C) and D) show a large variety of sizes of the rods.

larger rods seen in image C) are the original rods of the core sample. The compound surrounding these are the thinner and shorter rods observed in image D). Neodymium has been reported to influence the size of $NaYF_4$, making the particles smaller [45], therefore in image D) the rods are probably $NaYF_4$:Nd. Images C) and D) do not show the characteristic cubes of NaF, but the diffractogram in Figure 35 shows that there is NaF present in the sample.

In Figure 34 the SEM images of the sample prepared at 210^0C is presented. Images A) and B) are of the core-shell sample, whereas images C)-F) are of the core sample. Image 36 B) clearly shows the hexagonal structure of the rods. Figure 34 E) of the core sample is quite similar to Figure 26 of the first batch of method C, unfortunately there was some drifting of the electron beam.

It is remarkable in 36 A) and C) that the rods are aligned on all of the sides of the two cubes in the middle of the image. 36 D) shows that there are also varying diameters of the rods, and by 36 F) it is possible to estimate the length of the rods to be 1-1.2µm. What Figure 34 also illustrates is how little information is given by just showing the micrograph of one rod, such as is the case for the base article of method A [8].

Compared to the batch synthesised at 190^0C in Figure 33, the core-shell samples of the 210^0C batch seem more successful. This is primarily because the core-shell images are very similar to the core samples, and although there are rods of varying sizes there are not the very short or thin particles as seen in Figure 33 D). As opposed to the core-shell particles of method B, the size distribution does not exclude the presence of core-shell structures. According to the diffractogram in Figure 36, the phases present are still β-$NaYF_4$ and NaF.

To investigate the presence of a shell further, the samples were characterized by TEM and XPS. The results of these are shown in Figure 35 and Figure 37. The two techniques combined indicate that there is a core-shell structure and that there is neodymium present in the particles.

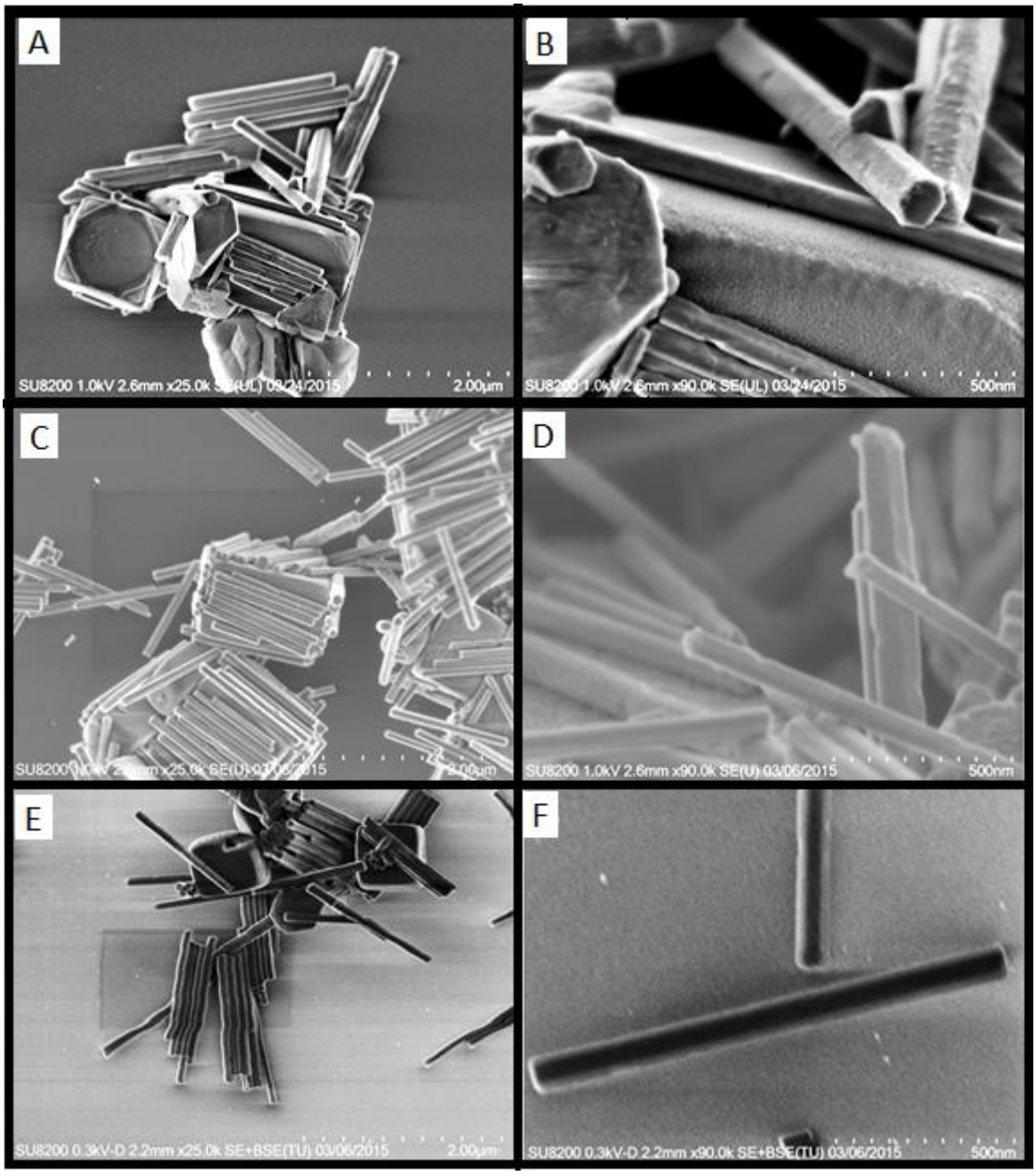

Figure 34 A) and B) are SEM images in deceleration mode of the core-shell sample synthesized at 210^{0}C. B) is a magnification of an area of A) showing that the rods are hexagonal. C) to F) are images of the core sample that was used as precursor for the core-shell sample. There are several similarities between the images A) and C) and B) and D). E) shows the similarity to the standard sample of method C and F) gives an indication of the size of the rods.

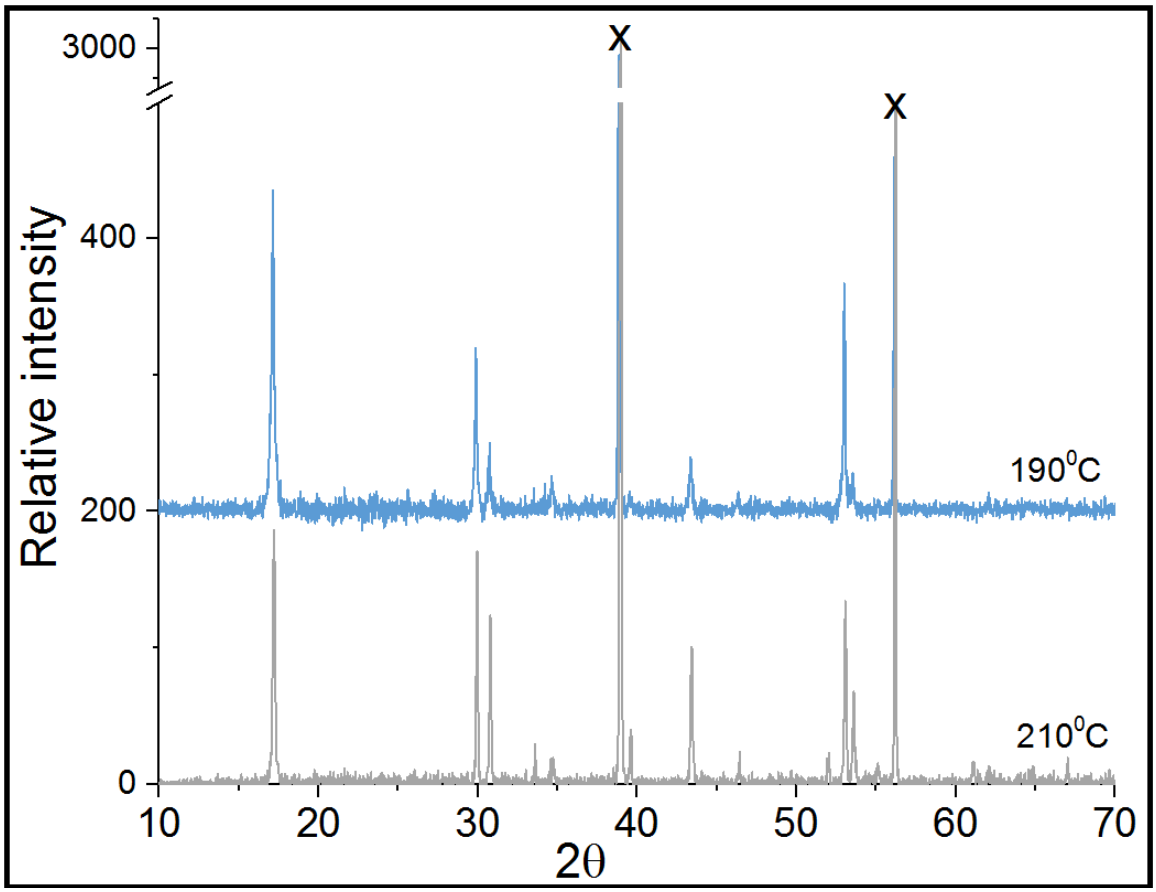

Figure 36 Diffractograms of the two core-shell samples made at 190°C and 210°C. Both show the presence of β-$NaYF_4$ as well as NaF marked by X.

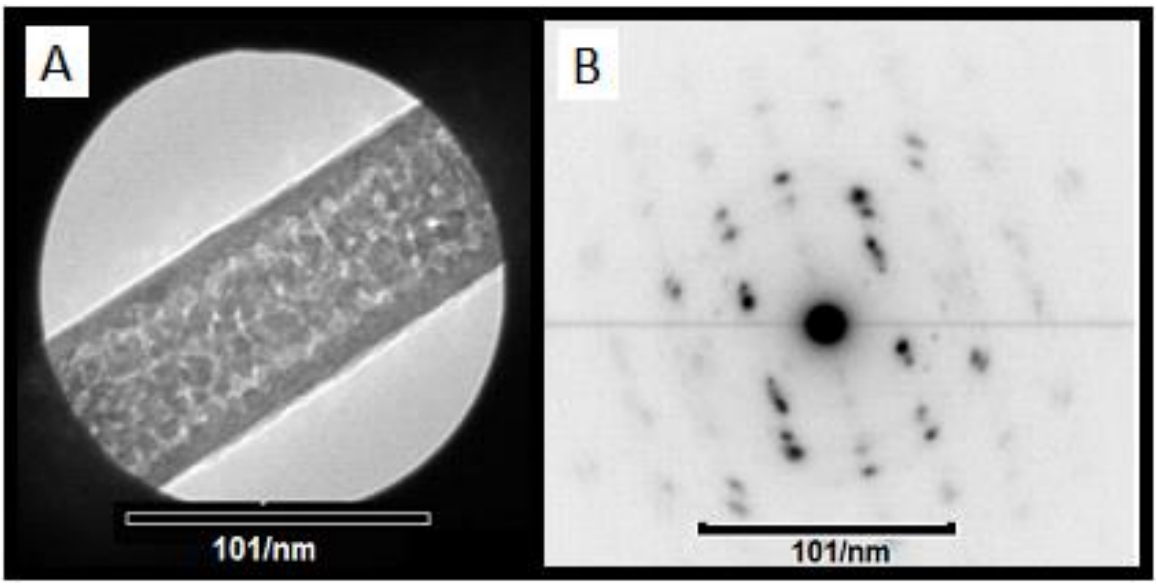

Figure 35 A) TEM image taken in STEM mode of the core-shell sample synthesised at 210°C. B) Diffractogram of the area of the rod shown in A). The two images support that there is a core-shell structure.

The STEM image in Figure 35 gives the first indication of a core-shell structure of the rods, seeing as there is a difference in contrast of the middle of the rod and the sides. The diffractogram in the same figure supports the assumption that the rod has been coated by an epitaxial layer. That is because the diffraction spots seem to be double and indicate that the diffraction comes from two crystals with different lattice parameters [47]. If there is a $NaYF_4$:Yb,Er@$NaYF_4$:Nd structure, then the diffraction pattern of both $NaYF_4$ hosts would be similar, however due to the size of the dopant ions the lattice parameters may differ.

The atomic percentages of the various elements in the core and core-shell samples given by the XPS measurements are shown in Table 13. The ratios of Na and Y to F do not correspond to 2:4 as it should for $NaYF_4$. A primary explanation for this is that the XPS measurements are taken for the entire sample and are therefore also averaged between the $NaYF_4$ rods and the NaF cubes. That might also explain the excess sodium compared to yttrium present. However, by taking the value of Y as the reference to how much $NaYF_4$ is present, the amount of F is still too low to be explained by the combined presence of $NaYF_4$ and NaF.

Sample	Na	Y	F	Nd
C_standard	32	12	56	-
C_core-shell	32	14	53.5	0.5
C_190_24h	38	8	54	-
C_190_24h_shell	27	14.5	58	0.5

Table 13 Atomic percentages of the various elements in the samples given by the XPS measurements

In Figure 37 the full XPS spectrum of the core and core-shell samples of method C (210^0C) is compared. A significant feature of the two spectra is that the one for the core-shell sample has a higher background signal than that of the core sample. This is often a feature of surface contamination, but for these samples it can be an indication of a core-shell structure [48]. Furthermore the core-shell shows a significant peak of Nd as opposed to the core sample, which is also reflected in Table 13.

Unfortunately none of the samples show visible UC by excitation at 808 nm, and the observed core-shell structure might be from oxygen contamination [14]. The core-shell samples did show UC at 980 nm as with the core samples.

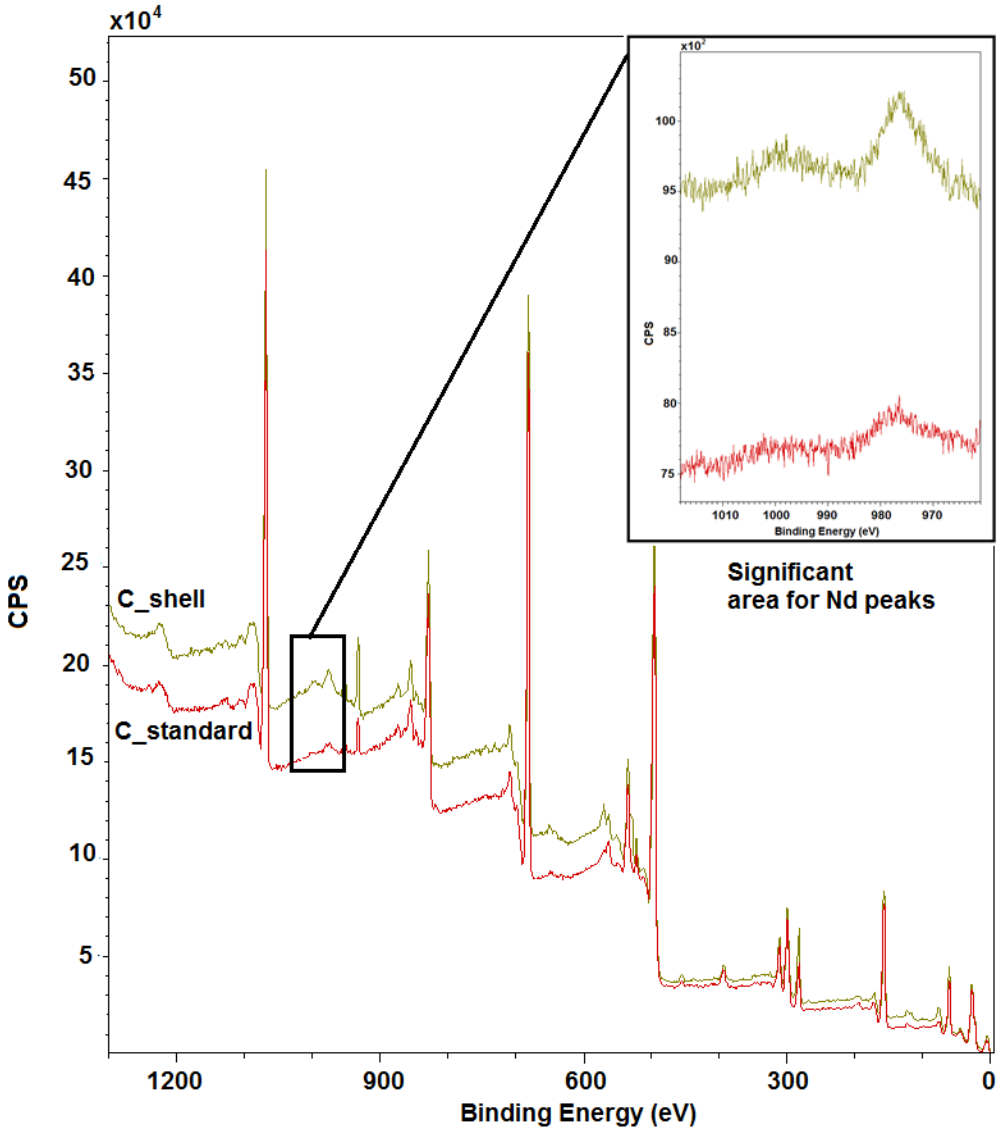

Figure 37 EDS spectra of core and core-shell structured samples made by method C at 210^{0}C for 24h, with an insertion of the specific area for the typical binding energy of Nd^{3+} which shows a significant difference between the standard sample and the core-shell structured sample.

4.4. LUMINESCENT PROPERTIES OF METHODS A-D

Figure 38 shows the luminescent spectrums obtained for each of the standard samples of methods A-D. Images A)-D) corresponds to methods A-D respectively. However, by comparing Figure 40 to the images of Figure 14 it is clear that the two peaks observed in 40 A)-D) around 540 and 600 nm are not related to the particles. The results in Figure 38 show that only methods A and D showed UC. From visible observations this is not true, as summarized in Table 14, all of the samples presented in section 4.1 show a visible green light when excited by 980 nm laser. Method D showed the best UC, which could be expected by the XRD and SEM results indicating a uniform and highly crystalline sample.

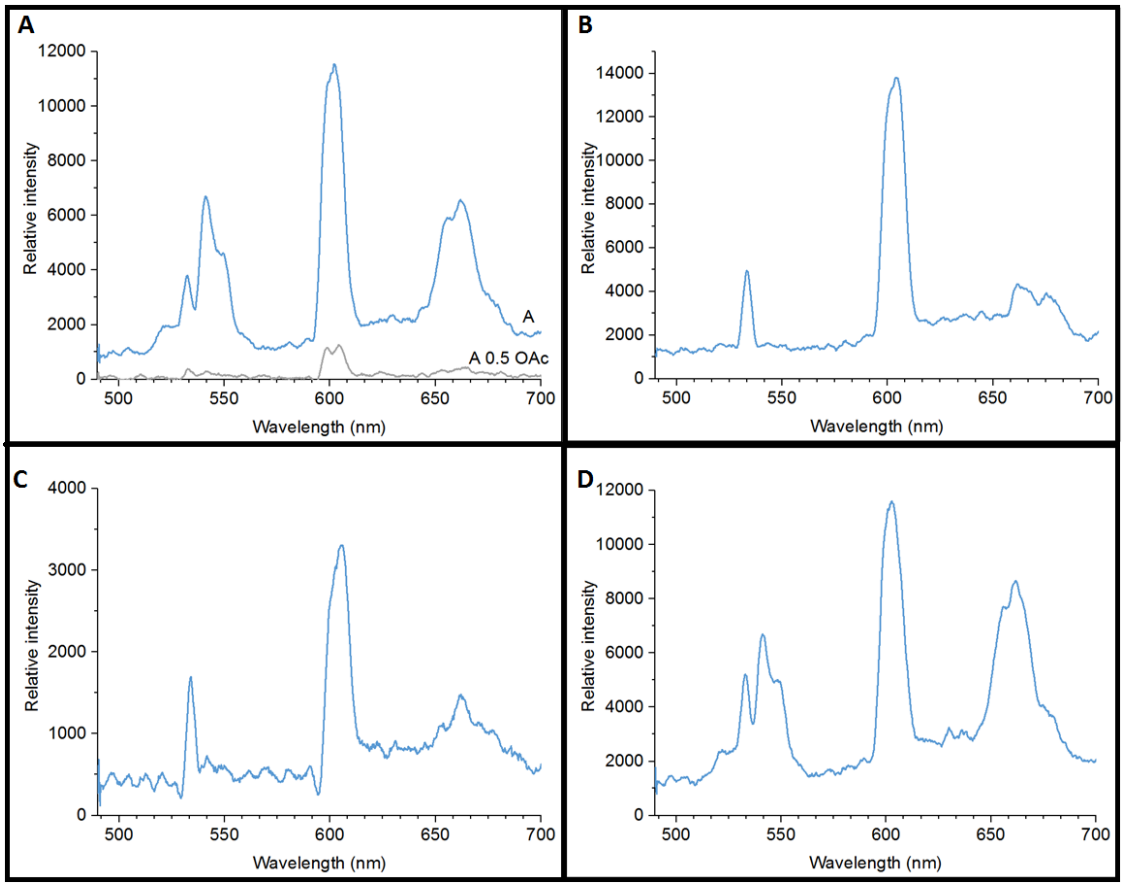

Figure 38 Luminescent measurements of the standard sample of each of the methods A-D. Images A)-D) corresponds to methods A-D respectively. The differnce between '*A*' and '*A 0.5OAc*' in image A) is the amount of surfactant used.The two peaks around 540 and 600 nm are not related to the particles as these are also observed for pure ethanol.

Following is a proposed explanation of this observation. Several setups for measuring the luminescent properties of the particles were applied. In solution the particles would quickly sediment. This resulted in that the laser only excited the particles in one end of the cuvette and that the detector placed at right angles to the laser did not catch the green luminescence. Some of the scattering of the signal may also be caused by NaF in the samples. Several different cuvettes (with different widths) were used in order to decrease the path length of the signal, and eventually the setup in Figure 18 proved successful.

The peaks around 540 nm and 600 nm are not originating from the sample. As can be seen by comparison to the two spectrums obtained by measuring the signal of a cuvette filled with only EtOH and a clean glass plate, see Appendix C – Optical measurements, the peaks around 540 nm and 600 nm originates from the laser. If it had been known earlier that the laser also emitted light at these wavelengths and not only at 980 nm a band-pass filter would have been obtained and applied for the measurements.

Table 14 Overview of which samples show visible upconversion luminescence

Synthesis method	Temperature / ^{0}C	Surfactants	Shows visible luminescence at excitation of 980 nm
A	210	OAc	yes
	210	½ OAc	yes
	190	OAc	yes
	170	OAc	yes
	200	3OAc : 1OAm	yes
	200	2OAc : 1OAm	yes
B	210	OAc	yes
C	210	OAc	yes
	200	1OAc : 1OAm	yes
	190	OAc	yes
D	210	OAc	yes

The luminescent spectrum was also measured on dry samples. When using the setup of Figure 18 there was a problem of saturation of the signal due to the reflection of the laser. The reflected signal increased when going from a transparent glass plate to having a white surface made up of the particles. This is also the reason why the sensing elements presented in the next section were not further investigated with regards to the interaction between the chromophore and the UCPs.

4.5. THE SENSING ELEMENT

To produce a sensing element as the one by Wolfbeis et al. [2] the UCPs had to be incorporated in a film. By using an inorganic silica film it would be possible to develop the work of Magne Kringberg in our research group, as well as to try something completely new, seeing as the previous sensing elements containing UCPs are based on organic polymers.

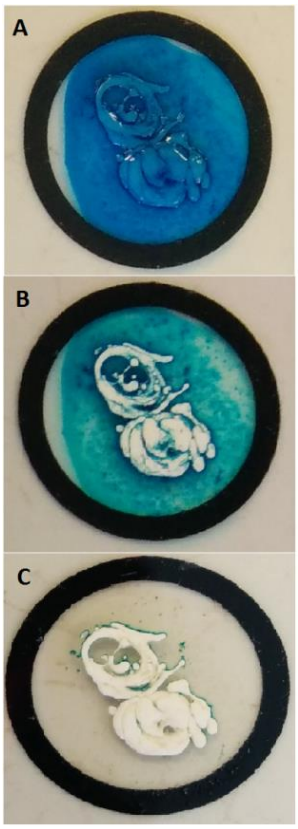

Figure 39 Photographs of BTB-TOA based sensing film with UCPs aggregated as a lump in the middle. A) immediately after deposition, B) after 3 days and C) 7 days

First BTB was applied because the absorption spectra overlap that of the emission of NaYF4:Yb,Er [8]. The chromophore is applied in the form of the ion pair BTB-TOA, which is necessary to incorporate it in the hydrophobic silica film.

As shown in Figure 39, the sensing element based on the ionpair BTB-TOA and UCPs was not a success. First of all the UCPs are not well mixed in the sol. The UCPs were dispersed in chloroform, but when added to the sol solution the UCPs formed a lump at the bottom of the plastic vial. The same happened when the UCPs were dispersed in cyclohexane.

Figure 42 shows the result when the sol containing UCPs was dropped on a microscope glass slate. Images A)-C) show the development of the film over time. This shows that the film in itself was not a success independent on the solubility of the UCPs. A) is directly after the deposition, B) is after a couple of days and after a week image C) shows that the sol is mostly evaporated. This means that the sol-gel network of the film was probably not formed at all, and is probably due to the excess solvent present in the sol.

Figure 40 is more promising and is consistent with Kringberg's results. He found that a sol-gel based on ODAOH-TMOS was better than the one based on TOAOH. By forming

the ionpair with ODA-TMOS instead of TOA he found that the chromophore was better incorporated in the gel. Cresol purple (CP) can also be used as chromophore for detecting changes in CO2 concentration. Furthermore its colour range is suitable for the filtering effect of the signal given by the UCPs. Figure 40 shows the result of incorporating CP-ODAC-TMOS in the gel. The film stayed unchanged for several weeks stored at room temperature. When placed in a 0.1 M solution of sodium bicarbonate the film gradually changed colours from purple to red and eventually yellow, also shown in Figure 40. The sensing element was sensitive towards CO_2 and regained the purple colour in a matter of seconds after being taken out of the solution.

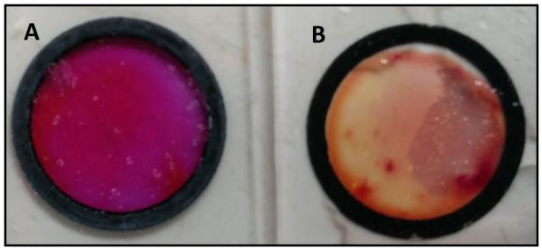

Figure 40 Photographs of CP-ODAC-TMOS based sensing film after 60 days. A) Purple and B) Orange and yellow after being dipped in $NaHCO_3$ (aq) solution. In less than a minute B) in standard atmosphere turns the same colour as A).

Due to the poor luminescent signal of the UCPs as shown in the previous section, as well as the poor solubility of the UCPs in the film, a sensing element with UCPs and CP was not synthesized. Further understanding of the UCPs is needed before the development of an inorganic sensing film that is compatible with the UCPs can be done systematically.

5. CONCLUSION

Microrods showing visible upconversion has been successfully synthesised by solvothermal synthesis. The various synthesis methods gave very different results in terms of the size and morphology of the particles, and is summarized in Figure 32 and

Table 12. The stoichiometry of the products can be questioned with regards to the EDS and XPS results, but based on the SEM images, XRD measurements and the visible UC it is very likely that β-$NaYF_4$:Yb,Er was formed.

The methods C and D developed for this project show more uniform particles than the methods A and B. The synthesis parameters of 210^0C and 24h for the autoclaves in the oven were found to be adequate to produce β-$NaYF_4$:Yb,Er. For method A, half the amount of surfactant produced smaller rods. Oleyl amine in combination with oleic acid (in the ratios used) was not successful in terms of controlling the morphology and size of the particles for method A or C. Pure oleic acid functioned for making near uniform particles, but does not contribute to form a colloidal solution. SEM images of methods A, C and D shows rods and cubes. The use of deceleration mode in SEM showed to be a powerful tool to produce clear micrographs. Diffractograms of all samples show β-$NaYF_4$, with the presence of NaF except for the samples synthesised by method B. It should be noted that electron beam-induced evaporation and re-deposition of the material was observed at large magnifications in the SEM.

All of the samples presented in the project showed visible upconversion in the form of green light. However, due to problems with dispersing the particles in solution and the wide range of wavelengths originating from the laser, not all samples showed clear results in the optical measurements, nor was there a strong visible light.

An attempt was made to synthesize core-shell particles by combining a heat-up method with the synthesis methods B and C. For method B a shell was probably not formed. There was a large difference between the SEM images of the core-shell particles synthesized by method C at 190^0C and 210^0C. The XRD and XPS results on the other

hand showed the same phases and the same elements present for the two samples. The 210^0C core-shell sample was also briefly investigated by TEM which showed double diffraction points and a different morphology of the middle and the sides of the rods. There are indications by TEM and XPS that there is a shell structure of the core-shell particles, however these are inconclusive results. The TEM measurements are particularly inconclusive due to poor statistics and lack of comparison with the core sample.

The production of a sensing element was not successful. The BTB-TOA system did not produce a durable sol-gel, nor were the UCPs compatible with the solution. The UCPs were not successfully dispersed in cyclohexane or chloroform and were therefore not compatible with producing a homogenous sensing film either, although this must be studied closer. A CP-ODAOH system formed a durable silica film that was sensitive to CO_2, and is a candidate for further testing together with the particles of method D.

6. FURTHER WORK AND FUTURE CHALLENGES

6.1. FURTHER WORK

There are many synthesis methods that are being studied with regards to phase, size and morphology of the $NaYF_4$ particles [7]. With regards to my project, I would focus on achieving a phase pure sample that forms a colloidal solution. In particular for better optical measurements, dispersion of the UCPs is critical. By having a dispersed solution the particles are more likely to be more evenly distributed in a gel as well. An aspect of this project that also needs further work is the compatibility of the UCPs with the sensing film.

A solution to these problems might be found by closer studies of the surfactant's interaction with the particles. For dry powder samples of the UCPs, Fourier transform infrared spectroscopy (FTIR) [43] and thermogravimetric measurements (TGA) can be applied. FTIR will give an indication as to whether the surfactant is present by showing peaks corresponding to the functional groups of the surfactant [43]. TGA can give an indication of the amount of surfactant by the weight loss as result of the treatment. Measuring the zeta-potential of the particles will also be of interest in terms of understanding the role of the surfactant. By further understanding the presence of the surfactant on the currently applied syntheses, it will be easier to further develop the synthesis method and hence the resulting particles.

Seeing as the novelty of this project would have been UC rods excited by IR laser at 800 nm, further work will not be carried out without looking into the development of the core-shell rods. The versatility of the heat-up method allows the shell to be synthesized by a different method, and so for instance the core particles of the solvothermal method may be added as reactants in a co-precipitation synthesis for making the core-shell particles.

Finally the optical measurements should be improved and the CO_2 sensing element finalized. A goal of a further work would be to synthesise a sensing element with UCPs excited at 800 nm, preferably with two shells to increase the UC efficiency by having the outermost shell inactive. The sensing element should also be characterized carefully in terms of sensitivity towards CO_2 and shelf life.

6.2. FUTURE CHALLENGES

A considerable future challenge for the field of UC is to combine material science, physics and chemistry. With the review article of 2004, Auzel [10] tried to establish a base of terms and expressions concerning UC. It can however be seen in various articles that these are not in place. There is not one standard method for synthesising UCPs, nor are the results of similar methods equal from group to group. This makes it difficult for research groups joining the field [7]. That is because they will have to do trials and error just to get the original material, before they can continue developing the research. Furthermore there are not standards for measuring and hence reporting the UC efficiency of the materials, so many research groups have had to duplicate previous works in order to compare the results with their own [5].

When it comes to optical sensors using UCPs, these are still dependent on chromophores that are sensitive to the analyte. Therefore, the reduced toxicity or increased photostability of UCPs compared to other compounds may not in reality lead to higher performance devices as these are still limited by the chromophores. Ways of omitting these obstacles should be investigated.

BIBLIOGRAPHY

1. Mills A. *Optical Sensors for Carbon Dioxide and Their Applications*. In: Sensors for Environment, Health and Security: Springer; 2009. p. 347-70.

2. Ali R, Saleh SM, Meier RJ, Azab HA, Abdelgawad II, Wolfbeis OS. *Upconverting nanoparticle based optical sensor for carbon dioxide*. Sensors and Actuators B: Chemical; 2010.

3. Lakowicz JR. *Principles of Fluorescence Spectroscopy*. 4th ed: Springer; 2010.

4. Andrea Cusano FJA, Michele Giordano, and Antonello Cutolo. *Optochemical Nanosensors.* Taylor & Francis; 2012.

5. Xu C ZQ, Liu H, Somesfalean G, Qian J, He S and Andersson-Engels S. *Upconverting nanoparticles for pre-clinical diffuse optical imagning, microscopy and sensing: Current trends and future challenges.* Laser Photonics Review; 2013.

6. Haase M, Schafer H. *Upconverting Nanoparticles.* Angew Chem Int Ed.; 2011.

7. Romanowski CF and Gainer M. *A review of synthetic methods for the production of upconverting lanthanide nanoparticles.* Journal of Innovative Optical Health Sciences; 2014.

8. Sun L-N, Peng H, Stich MIJ, Achatz D, Wolfbeis OS. *pH sensor based on upconverting luminescent lanthanide nanorods*. Chemical Communications; 2009.

9. Husing N and Schubert U . *Synthesis of Inorganic Materials*. Wiley-VCH Verlag & co; 2012.

10. Auzel F. *Upconversion and Anti-Stokes Processes with f and d Ions in Solids*. Chemical Reviews; 2004.

11. Dong H, Sun L-D, Yan C-H. *Basic understanding of the lanthanide related upconversion emissions.* Nanoscale; 2013.

12. Jing-Hui Zeng JS, Zhi-Hua Li, Ruo-Xue Yan and Ya-Dong Li. *Synthesis and Upconversion Luminescence of Hexagonal-Phase NaYF4:Yb,Er3+ Phosphors of Controlled Size and Morphology*. Adv Mater.; 2005.

13. Romanowski CF and Gainer M. *A review of synthetic methods for the production of upconverting lanthanide nanoparticles.* Journal of Innovative Optical Health Sciences; 2014.

14. Zhang F, Wan Y, Yu T, Zhang F, Shi Y, Xie S, et al. *Uniform Nanostructured Arrays of Sodium Rare-Earth Fluorides for Highly Efficient Multicolor Upconversion Luminescence.* Angewandte Chemie; 2007.

15. Xie X, Gao N, Deng R, Sun Q, Xu Q-H, Liu X. *Mechanistic Investigation of Photon Upconversion in Nd3+-Sensitized Core–Shell Nanoparticles.* Journal of the American Chemical Society; 2013.

16. Park YI, Kim JH, Bae YM, Byeongjun Y, Hyung MK, Hyo SP, Choi JS and Lee TK. *Comparative Study of Upconverting Nanoparticles with Various Crystal Structures, Core/Shell Structures, and Surface Characteristics*. J Phys Chem C.; 2013.

17. Gai S, Li C, Yang P, Lin J. *Recent Progress in Rare Earth Micro/Nanocrystals: Soft Chemical Synthesis, Luminescent Properties, and Biomedical Applications.* Chemical Reviews; 2014.

18. Chen X, Peng D, Ju Q, Wang F. *Photon upconversion in core-shell nanoparticles*. Chemical Society Reviews; 2014.

19. Wilhelm S, Kaiser M, Wurth C, Heiland J, Carrillo-Carrion C and Muhr V. *Water dispersible upconverting nanoparticles: effects of surface modification on their luminescence and colloidal stability.* Nanoscale; 2015.

20. Zhong Y, Tian G, Gu Z, Yang Y, Gu L, Zhao Y, et al. *Elimination of Photon Quenching by a Transition Layer to Fabricate a Quenching-Shield Sandwich Structure for 800 nm Excited Upconversion Luminescence of Nd3+-Sensitized Nanoparticles.* Advanced Materials; 2014.

21. Mader HS, Wolfbeis OS. *Optical Ammonia Sensor Based on Upconverting Luminescent Nanoparticles.* Analytical Chemistry; 2010.

22. Sun J, Zhang W, Du H, Yang Z. *Hydrothermal synthesis and the enhanced blue upconversion luminescence of NaYF4:Nd3+,Tm3+,Yb3+*. Infrared Physics & Technology; 2010.

23. Wu J, Qin Y. *Polymeric optodes based on upconverting nanorods for fluorescence measurements of Pb2+ in complex samples*. Sensors and Actuators B: Chemical; 2014.

24. Xie L, Qin Y, Chen H-Y. *Direct Fluorescent Measurement of Blood Potassium with Polymeric Optical Sensors Based on Upconverting Nanomaterials*. Analytical Chemistry; 2013.

25. Liu J, Lu L, Li A, Tang J, Wang S and Xu S. *Simultaneous detection of hydrogen peroxide and glucose in human serum with upconversion luminescence.* Biosensors and Bioelectronics; 2015.

26. Kringberg M. *Optical Sensors for Dissolved Carbon Dioxide*. Master Thesis. University of Oslo; 2014.

27. Fan Zhang JL, Shan J, Xu L and Zhao G. S*hape, Size and Phase-Controlled Rare-Earth Fluoride Nanocrystals with Optical Up-Conversion Properties*. Chem Eur J.; 2009.

28. Ding M, Yin S, Ni Y, Lu C, Chen D and Zhong J. *Controlled synthesis of β-NaYF4:Yb3+/Er3+ microstructures with morphology- and size-dependent upconversion luminescence*. Ceramics International; 2015.

29. Guo J, Ma F, Gu S, Shi Y and Xie J. *Solvothermal synthesis and upconversion spectroscopy of monophase hexagonal NaYF4:Yb3+/Er3+ nanosized crystallines*. Journal of Alloys and Compounds; 2012.

30. Gao D, Zhang X, Zheng H, Gao W and He E. *Yb3+/Er3+ codoped β-NaYF4 microrods: Synthesis and tuning of multicolor upconversion*. Journal of Alloys and Compounds; 2013.

31. Jiao Y, Gao X, Lu J, Chen Y, He W and Chen X. *Hydrothermal synthesis of the intense green photoluminescence of hexagonal phase NaYF4:Yb3+/Er3+ microcrystals.* Journal of Alloys and Compounds; 2013.

32. Wang Y, Gai S, Niu N, He F and Yang P. *Synthesis of NaYF4 microcrystals with different morphologies and enhanced up-conversion luminescence properties*. Physical Chemistry Chemical Physics; 2013.

33. Lin M, Zhao Y, Liu M, Qiu M, Dong Y and Duan Z. *Synthesis of upconversion NaYF4:Yb3+,Er3+ particles with enhanced luminescent intensity through control of morphology and phase.* Journal of Materials Chemistry C.; 2014.

34. Liu S, Wang G, Pan K, Li Y, Feng L and Tian C. C*olloidal lanthanide-doped NaLuF4:Ln3+ nanocrystals: Synthesis, energy transfer, and tunable luminescence properties.* Journal of Fluorine Chemistry; 2013.

35. Shen J, Chen G, Vu A-M, Fan W, Bilsel OS and Chang C-C. *Engineering the Upconversion Nanoparticle Excitation Wavelength: Cascade Sensitization of Tri-doped Upconversion Colloidal Nanoparticles at 800 nm*. Advanced Optical Materials; 2013.

36. Liu F and Wang X. *Recent advances in the chemistry of lanthanide-doped upconversion nanocrystals.* Chem Soc Rev.; 2009.

37. Chen G, Qiu H, Prasad PN and Chen X. *Upconversion nanoparticles: Design, nanochemistry, and applications in Theranostics.* Chemical Reviews; 2014.

38. Leng Y. *Materials Characterization*. John Wiley & Sons (Asia) Pre Ltd; 2008.

39. Brandon D. *Microstructural Characterization of Materials.* 2 ed. Wiley; 2008.

40. Ding M, Yin S, Chen D, Zhong J, Ni Y and Lu C. *Hexagonal NaYF4:Yb3+/Er3+ nano/micro-structures: Controlled hydrothermal synthesis and morphology-dependent upconversion luminescence.* Applied Surface Science; 2015.

41. Tilley RJD. *Understanding Solids*. John Wiley & Sons Ltd; 2004.

42. Ye X, Collins JE, Kang Y, Chen J, Chen DTN and Yodh AG. *Morphologically controlled synthesis of colloidal upconversion nanophosphors and their shape-directed self-assembly*. Proceedings of the National Academy of Sciences; December 28th 2010.

43. Mourdikoudis S, Liz-Marzán LM. *Oleylamine in Nanoparticle Synthesis. Chemistry of Materials*. Chem. Mater.; 2013.

44. Chang H, Xie J, Zhao B, Liu B, Xu S, Ren N, et al. *Rare Earth Ion-Doped Upconversion Nanocrystals: Synthesis and Surface Modification.* Nanomaterials; 2014.

45. Xian Chen DPaFW. *Tuning NaYF4 Nanoparticles through Alkaline Earth Doping. Nanomaterials*. Nanomaterials; 2013.

46. Lisjak D, Plohl O, Ponikvar-Svet M, Majaron B. *Dissolution of upconverting fluoride nanoparticles in aqueous suspensions*. RSC Advances; 2015.

47. Personal communication with Prytz Ø., University of Oslo 2015.

48. Personal communciation with Jørgensen S., University of Oslo 2015.

APPENDIX A - PRECURSORS

Overview of amount of precursors dissolved in water for each of the three synthesis methods

Chemical	Molar Mass /gmol^{-1}	Amount for method A /g	Amount for method B /g	Amount for method C /g	Volumetric flask /ml
$Er(NO_3)_3 \cdot 5H_2O$	443.35	0.887	1.783	0.887	10
$Nd(NO_3)_3 \cdot 6H_2O$	438,4	-	3.960	0.900	10
$Yb(NO_3)_3 \cdot 5H_2O$	449.13	0.908	2.828	0.908	10
$Y(NO_3)_3 \cdot 5H_2O$	383.01	3.840	6.135	3.840	20
NaF	41.99	4.196	0.240	4.196	100

APPENDIX B – EXTRA RESULTS OF METHOD B

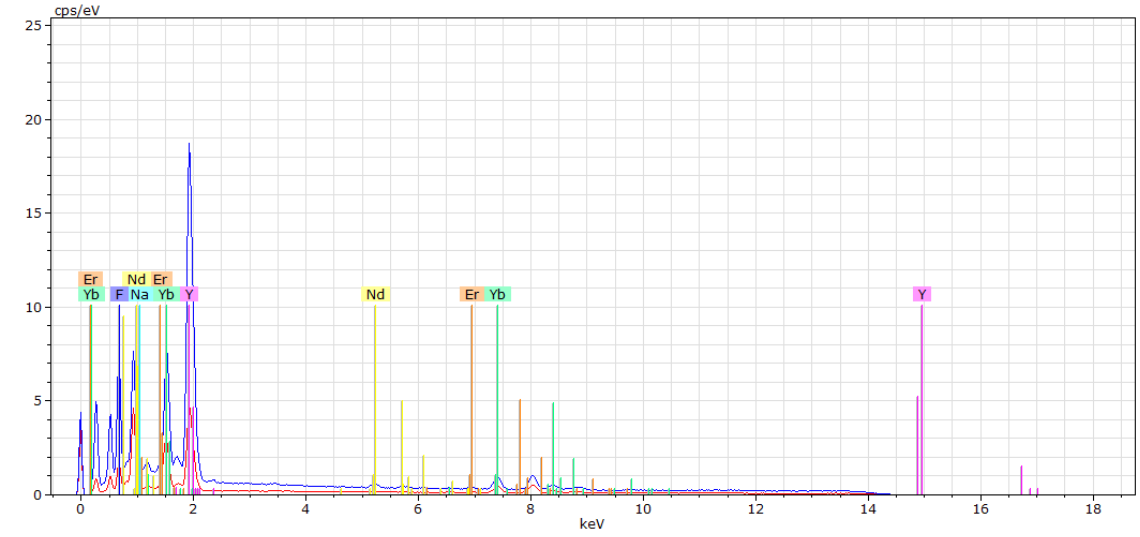

Atomic percent (%)

Spectrum	F	Na	Y	Nd	Er	Yb
NaYF-2310	47.72	3.68	35.19	-	2.29	11.12
NaYFNd-1011 16	56.27	0.00	35.59	0.76	1.24	6.13
Mean value:	52.00	1.84	35.39	0.76	1.77	8.62
Sigma:	6.05	2.60	0.29	0.00	0.74	3.53
Sigma mean:	4.28	1.84	0.20	0.00	0.52	2.50

Illustration 1 EDS spectrum by SEM of method B samples core and core-shell

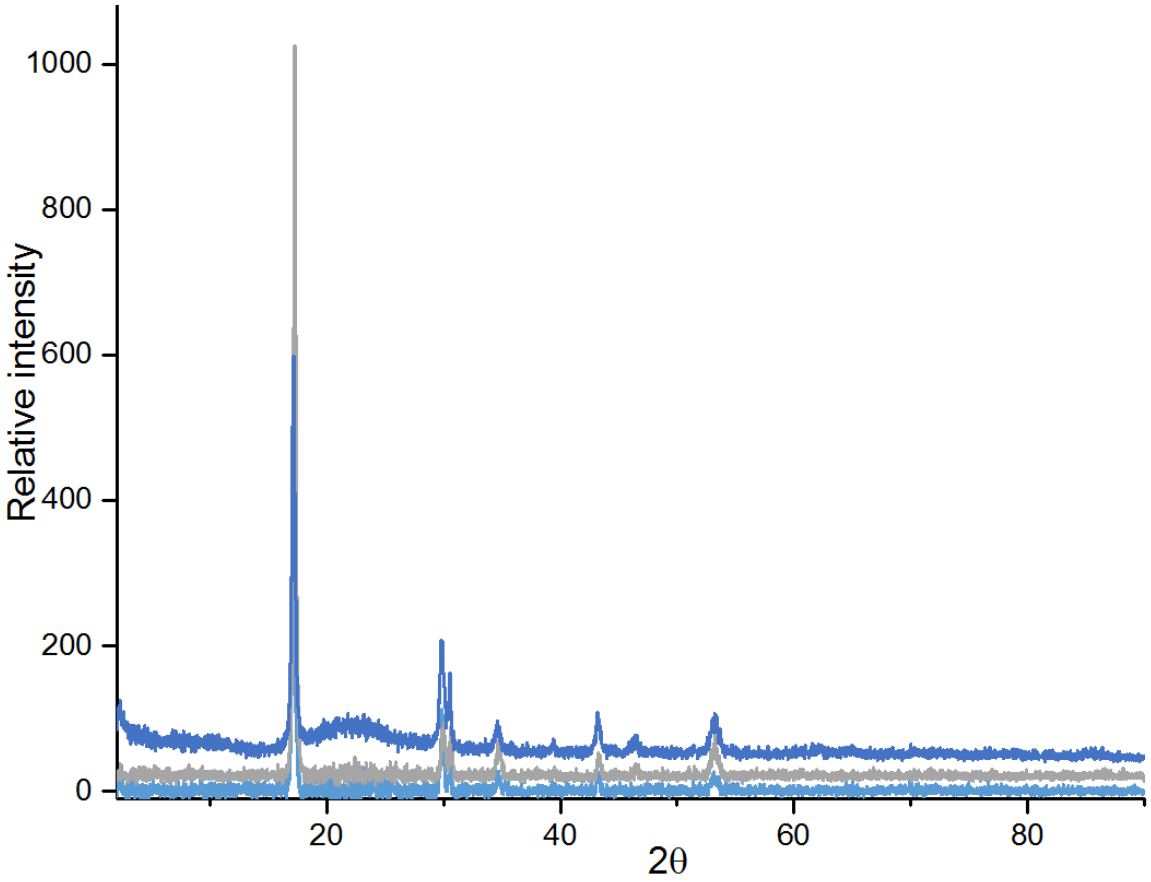

Illustration 2 Diffractograms of batches 1 through 3 of method B, all showing pure β-$NaYF_4$

APPENDIX C – OPTICAL MEASUREMENTS

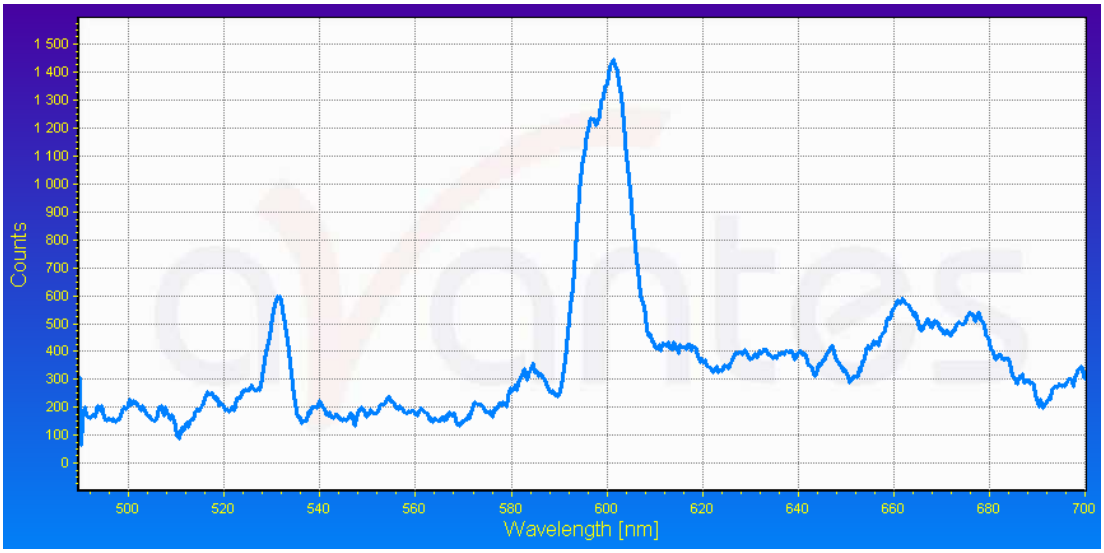

Illustration 3 Luminescent spectrum of cuvette with ethanol only

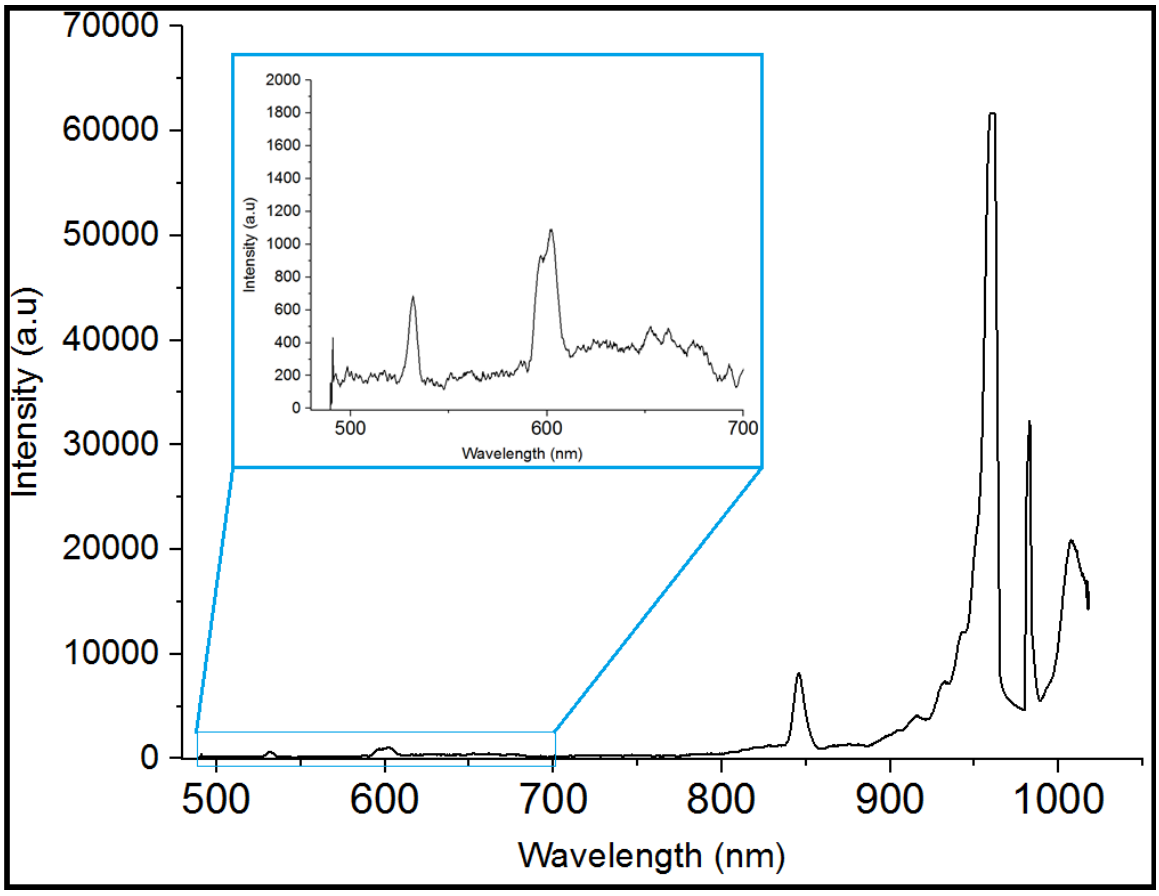

Illustration 4 The signal of the 980 nm laser reflected by a clean glassplate

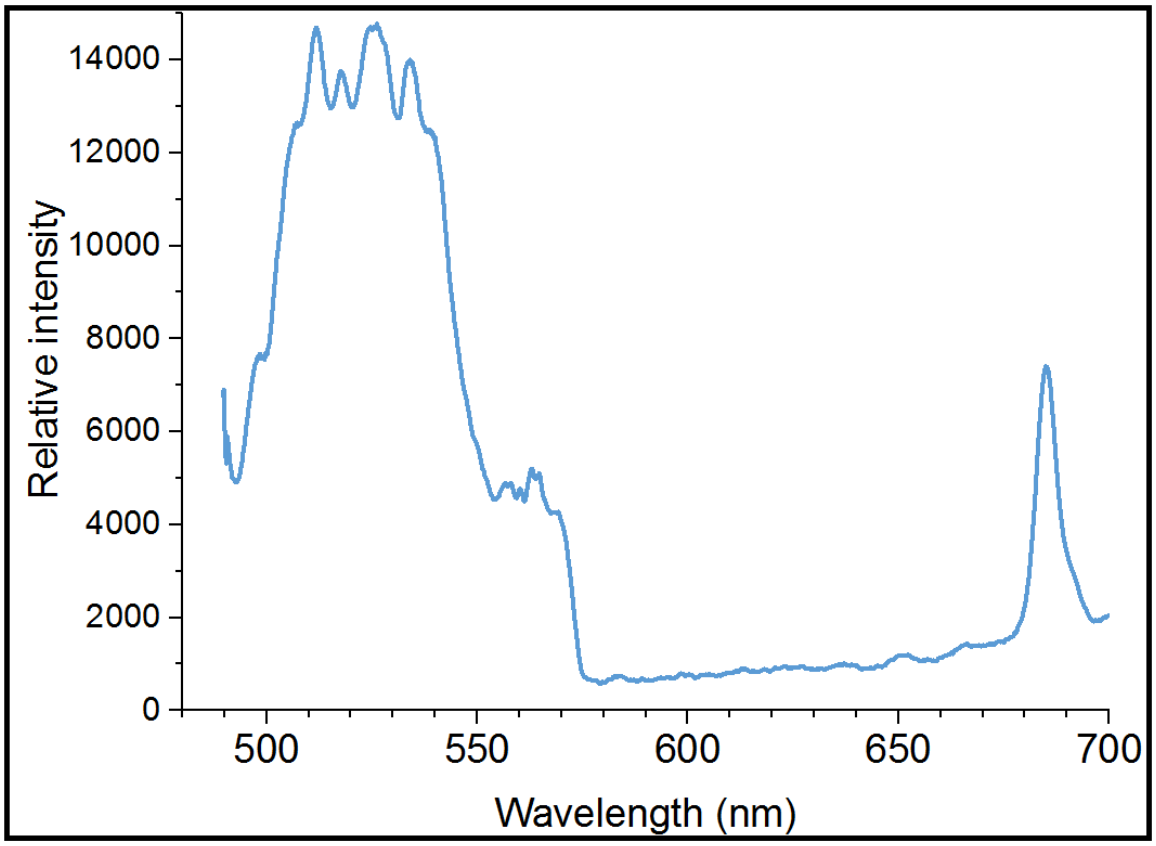

Illustration 5 Signal of the 808 nm laser reflected off a glass plate

APPENDIX D – THE LASERDRIVE

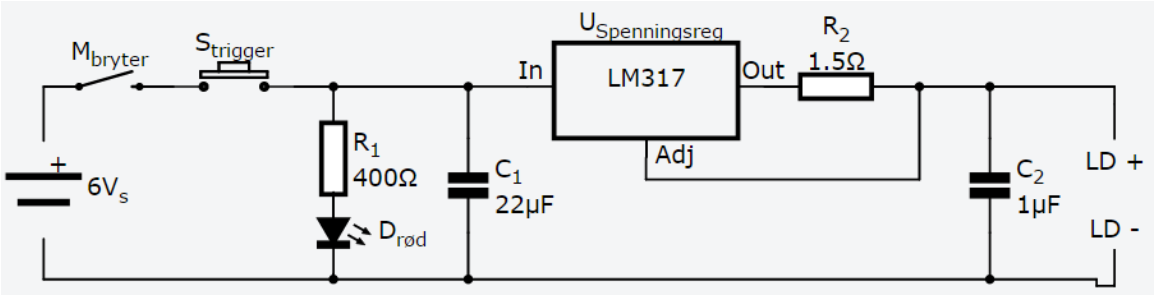

Illustration 6 Scheme of the circuit of the laser drive

APPENDIX E – THE COMMERSIAL SAMPLE

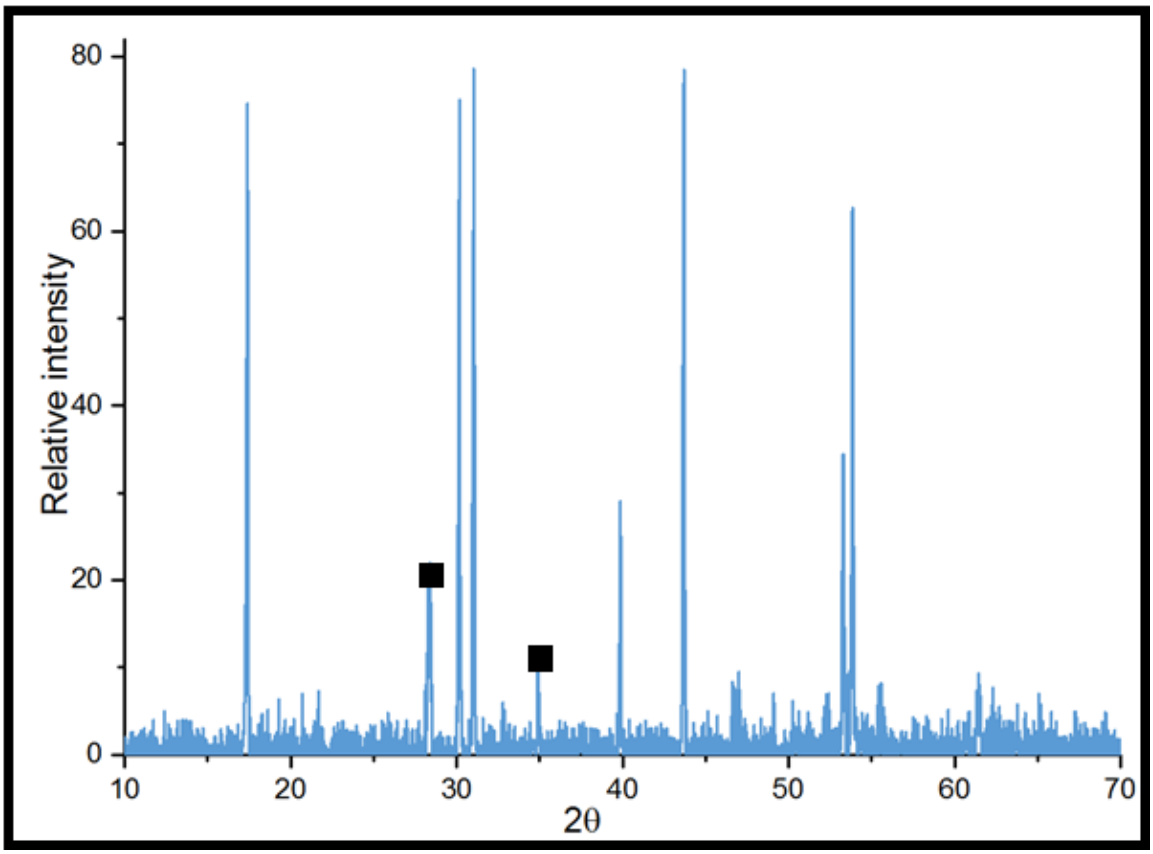

Illustration 7 Diffractogram of the commercial sample which clearly shows that it has both α- and β-$NaYF_4$ present.